*Meteoritics & Planetary Science* 38, Nr 1, 13–33 (2003)
Abstract available online at http://meteoritics.org

# On estimating contributions of basin ejecta to regolith deposits at lunar sites

Larry A. HASKIN*, Billy E. MOSS, and William B. McKINNON

Department of Earth and Planetary Sciences and McDonnell Center for the Space Sciences,
Washington University, One Brookings Drive, St. Louis, Missouri 63130, USA
*Corresponding author. E-mail: lah@levee.wustl.edu

*(Received 12 March 2002; revision accepted 3 October 2002)*

**Abstract**–We have developed a quantitative model for predicting characteristics of ejecta deposits that result from basin-sized cratering events. This model is based on impact crater scaling equations (Housen, Schmitt, and Holsapple 1983; Holsapple 1993) and the concept of ballistic sedimentation (Oberbeck 1975), and takes into account the size distribution of the individual fragments ejected from the primary crater. Using the model, we can estimate, for an area centered at the chosen location of interest, the average distribution of thicknesses of basin ejecta deposits within the area and the fraction of primary ejecta contained within the deposits. Model estimates of ejecta deposit thicknesses are calibrated using those of the Orientale Basin (Moore, Hodges, and Scott 1974) and of the Ries Basin (Hörz, Ostertag, and Rainey 1983). Observed densities of secondary craters surrounding the Imbrium and Orientale Basins are much lower than the modeled densities. Similarly, crater counts for part of the northern half of the Copernicus secondary cratering field are much lower than the model predicts, and variation in crater densities with distance from Copernicus is less than expected. These results suggest that mutual obliteration erases essentially all secondary craters associated with the debris surge that arises from the impacting primary fragments during ballistic sedimentation; if so, a process other than ballistic sedimentation is needed to produce observable secondary craters. Regardless, our ejecta deposit model can be useful for suggesting provenances of sampled lunar materials, providing information complementary to photogeological and remote sensing interpretations, and as a tool for planning rover traverses (e.g., Haskin et al. 1995, 2002).

## INTRODUCTION

This paper considers impact ejecta modeling from the point of view of a geochemist or petrologist who wishes to constrain hypotheses of the place of origin of sampled or remotely sensed materials, or who wishes to estimate the probability of encountering material from a particular source along a traverse designed to answer a specific geologic question. We offer a way to estimate thicknesses of ejecta deposits that have been produced by basin-forming and large crater-forming events at a lunar site. Here, the term "ejecta deposit" is used to mean the mixed deposit that is produced when ejecta from a primary cratering event strike the planetary surface, not just those ejecta themselves. The model set forth in this paper is based on previously developed crater scaling and ejecta models (Housen, Schmitt, and Holsapple 1983; Melosh 1989; Holsapple 1993; O'Keefe and Ahrens 1993) and on formation of ejecta deposits by ballistic excavation and sedimentation (Oberbeck 1975; Oberbeck et al. 1974, 1975; Morrison and Oberbeck 1975, 1978; Moss and Haskin 1994). The model applies mainly to deposits from the outer edges of continuous ejecta deposits and beyond. Our results provide a test for the reasonableness of a particular hypothesis of origin of a material encountered in a deposit. The Imbrium impact event is used as an example.

The model estimates the surface density of ejecta from the chosen primary crater that fall upon a location of interest, calculates the size distribution of the ejecta fragments arriving at the location, and then estimates the areal density of secondary craters of each size. The model uses secondary cratering efficiencies to estimate the quantity of local substrate excavated by the ejecta as the secondary craters are produced. From these results, the model estimates the probabilities of different thicknesses of the ejecta deposits and of different proportions of primary ejecta and the substrate they contain at that location. The model thus estimates the variability of both deposit thickness and the fraction of primary ejecta to be expected over a local area containing the location of interest. The modeling here is based on vertical or near-vertical *primary* impacts. It ignores physical effects of

pre-existing topography on the development of an ejecta deposit. It estimates only average properties of ejecta deposits, and does not consider effects of discontinuous ejecta, such as rays.

We acknowledge the importance of remote observations and geologic interpretation of data therefrom. Images, topographic and gravity data, and spectra reveal much about a site of interest. Expectations based on modeling provide information complementary to such observations and may be of value in explaining them and looking beyond them.

The principal basis for the modeling is contained in the summary discussion of ballistic sedimentation in Oberbeck (1975). In brief, when a projectile at hypervelocity (~10–15 km/sec at the Moon) impacts a planetary surface, it produces a primary crater whose ejecta fragments follow ballistic trajectories until they impact the surface. We will call those fragments "PriFrags" to distinguish them from the abundant ejecta from secondary craters. Our model takes into account their individual effects. PriFrags of interest from lunar basin-sized impacts have velocities up to ~2.3 km/sec (any with higher velocity escape lunar gravity). PriFrags form secondary craters when they drop back onto the surface. We will refer to the materials of the surface prior to arrival of any PriFrags as "substrate." PriFrags have a horizontal momentum component. Part of that momentum is transferred to the substrate ejected as the secondary craters form. The resulting motion produces a surge radially downrange from the site of the primary impact. This surge obscures smaller secondary craters and further mixes the PriFrags with substrate. Although our model treats mixing on a gross scale, on a smaller scale, blocks of primary ejecta may survive this process intact, as may batches of excavated substrate. Thus, collected lunar samples may be ejected basin material, local substrate, or a combination of both. The extent of macro-scale mixing of PriFrags with substrate is described by an excavation efficiency (the $\mu$ of Oberbeck et al. 1975), defined as the mass of excavated substrate divided by the mass of the impacting fragment that excavated it. Other mechanisms such as vaporization and spallation remove some of the material lost from the primary crater (e.g., Melosh 1989, Section 6.4), but are ignored here.

First, we show on the basis of Copernicus secondary crater statistics that estimates of average properties of ejecta deposits may better approximate crater distributions far beyond the region of continuous deposits than might be expected. Next, we present the model, followed by a demonstration of the nature of its results, emphasizing the variation of ejecta deposit properties to be expected in the vicinity of a site of interest. We then compare results from the model against observed deposit thicknesses and crater densities and use the comparison to calibrate the efficiency of excavation by the overlapping secondary craters that affect a given location. Finally, we show how sensitive the model predictions are to changes in the values of the various input parameters.

## CRATER DENSITY STATISTICS; DEVIATIONS FROM AVERAGE VALUES

The model presented here estimates the average properties of ejecta deposits at distances out to many transient crater radii. How valuable are such average estimates likely to be, given that beyond the continuous deposits, ejecta deposits are stochastically distributed, partly in ray-producing filaments? We attempt to gain some sense of this by analyzing the number of visible secondary craters in ejecta deposits of the 93 km diameter crater Copernicus. We measured the surface density of craters in the northern half of the Copernicus secondary crater field over a distance of ~4.7 to 6.8 transient crater radii (145–210 km) from the crater center, the transient crater radius taken to be ~2/3 of the present radius of 93 km (Melosh 1989, p. 144). This region is shown in Lunar Orbiter photos IV-121$H_2$ and IV-126$H_2$. We found that ~0.5 km was the lower limit of resolution for identifying and counting secondary craters, in agreement with estimates from Pieters et al. (1985), whose work used the same images. Copernicus secondary craters were identified according to the distinguishing features outlined by Wilhelms, Oberbeck, and Aggarwal (1978). We were unable to distinguish individual secondary craters at distances closer than ~4 transient crater radii from the crater center, and we were not confident of our ability to distinguish between primary and isolated secondary craters at distances greater than ~7 transient crater radii.

Images of secondary craters 0.5 km diameter and larger were traced onto mylar film. The resulting crater field was divided into a grid of 15 × 15 km squares, which we will call "squares of interest" (SOIs). (Relative to the size of the Copernicus transient crater, the 15 × 15 km SOIs are slightly smaller than the 100 × 100 km SOIs we will use later in relation to basin-forming transient craters.) The number of craters within each square was determined. Semicircles with radii corresponding to distances of 145, 178, 194, and 210 km (between 4.7 and 6.8 transient crater radii) from the center of Copernicus were drawn through the field of squares. The number of Copernicus secondary craters in each square intersected by each semicircle is given in Table 1. We also determined the number of secondary craters in smaller (7.5 × 7.5 km) SOIs intersected by the semicircles. These are model-independent data that provide a quantitative measure of secondary crater densities as a function of distance from the primary crater, the extent to which those crater densities vary from average values, and how this variability changes with distance from the site of the primary impact.

Histograms of crater density are shown in Fig. 1, as numbers of secondary craters ≥0.5 km per SOI. Crater counts as a function of distance from the center of Copernicus are shown in Fig. 2. (The model results included in Fig. 2 are discussed in a later section.) Nearly 90% of the 15 × 15 km SOIs comprising the ring at 145 km have secondary crater

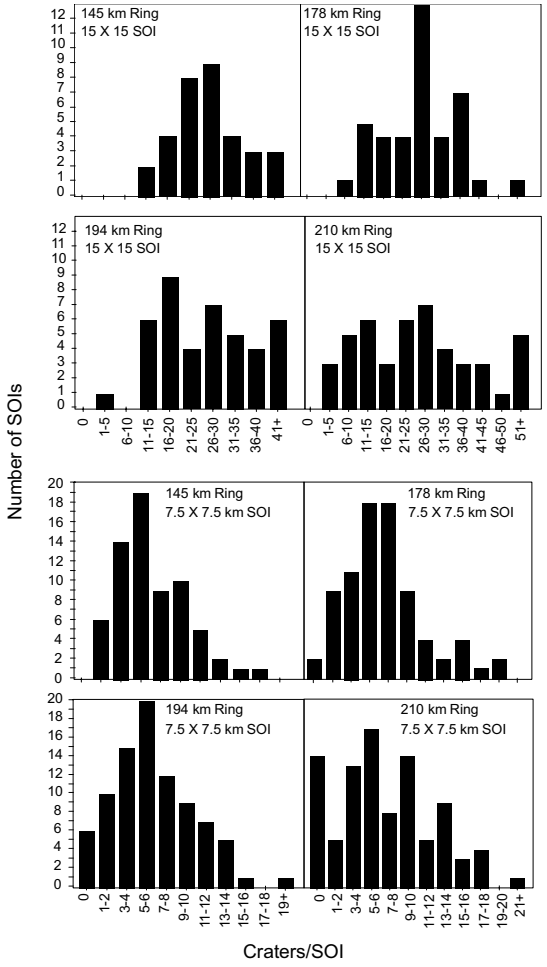


Fig. 1. Histograms are shown for the number of secondary craters with diameters ≥0.5 km in the northern half of the Copernicus crater field for half-rings of Squares of Interest (SOIs) at different distances from the center of the primary crater (145, 178, 194, and 210 km; i.e., ~4.7 to ~6.8 transient crater radii). SOIs of 15 km × 15 km and of 7.5 km × 7.5 km in size were used. Note that within the range of distances observed, no 15 km × 15 km SOI failed to have at least one observable secondary crater.

densities within ±50% of the average for those SOIs (i.e., within the range 27.5 ± 13.8 craters/SOI). This fraction decreases with distance from the crater, but is still 65% at 210 km. These results are consistent with the qualitative observation that farther from Copernicus there are larger areas without obvious secondary craters. Even at the greatest distance analyzed, 210 km (6.8 transient crater radii), no 15 × 15 km SOI was devoid of Copernicus secondary craters. The much smaller 7.5 × 7.5 km SOIs (Table 1) yield correspondingly higher proportions of SOIs outside the range of ±50% on average. We note that Copernicus secondary crater densities reported by Gault et al. (1975; Fig. 11) are only 0.2–0.3 times those reported here.

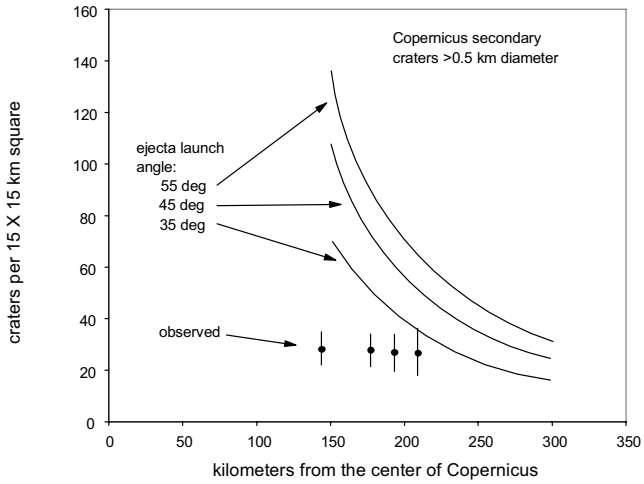


Fig. 2. The average numbers of Copernicus secondary craters 0.5 km in diameter per 15 km × 15 km SOI are shown as a function of distance from the center of Copernicus. Error bars are one sample standard deviation but, because the distributions are not Gaussian, they are only rough indicators of the spread. The numbers of craters estimated by the model are shown for three ejection angles.

The Copernicus results suggest that, for distances from the crater rim up to at least ~7 transient crater radii from the center of the primary impact (the distance beyond which we could no longer distinguish secondary craters with confidence), the majority of SOIs have secondary crater counts within ±50% of the average count for that distance. This modest amount of variability from SOI to SOI suggests that average modeled properties may usefully apply to actual results. This conclusion, based only on the observed distribution of Copernicus secondary craters, is independent of any modeling. The variability in crater counts becomes greater as the distance from the primary crater increases and the number of contributing rays decreases. We assume that the more abundant, small PriFrags that produce unobservably small secondary craters have the same areal distribution as the larger PriFrags. The spread of the smaller PriFrags could be broader and more nearly uniform than that for the larger PriFrags, but we have no observational evidence to support this possibility. We had initially presumed that observations of variability made on secondary crater densities would also apply to ejecta deposit thicknesses, but results of the modeling indicate that ejecta deposit thicknesses may not be closely connected to observable secondary crater densities, as discussed below.

## MODELING OF EJECTA DEPOSIT PROPERTIES

Because we have combined several modeling procedures to obtain estimates of deposit thickness and fractions of PriFrags in deposits, we present the basis for our calculations in detail in this section. The values of constants used in most of the calculations are given in Table 2, and the overall

Table 1. Craters counts in individual SOIs in half-rings north of Copernicus.
km = distances from center of Copernicus to center of SOIs; SOIs are counted from west to north to east.

| 15 km × 15 km SOIs | | | | | 7.5 km × 7.5 km SOIs | | | | | 7.5 km × 7.5 km SOIs | | | | |
|---|---|---|---|---|---|---|---|---|---|---|---|---|---|---|
| km | 145 | 178 | 194 | 210 | km | 145 | 178 | 194 | 210 | km | 145 | 178 | 194 | 210 |
| SOI # | #crat | #crat | #crat | #crat | SOI # | #crat | #crat | #crat | #crat | SOI # | #crat | #crat | #crat | #crat |
| 1 | 16 | 11 | 17 | 16 | 1 | 4 | 0 | 2 | 3 | 48 | 7 | 16 | 12 | 11 |
| 2 | 35 | 11 | 11 | 11 | 2 | 6 | 4 | 6 | 7 | 49 | 6 | 5 | 0 | 13 |
| 3 | 14 | 26 | 11 | 10 | 3 | 8 | 1 | 3 | 1 | 50 | 6 | 4 | 2 | 9 |
| 4 | 34 | 40 | 14 | 5 | 4 | 4 | 2 | 5 | 0 | 51 | 4 | 8 | 4 | 3 |
| 5 | 28 | 20 | 21 | 13 | 5 | 1 | 6 | 4 | 6 | 52 | 6 | 6 | 5 | 4 |
| 6 | 21 | 33 | 28 | 42 | 6 | 4 | 12 | 0 | 0 | 53 | 2 | 8 | 9 | 0 |
| 7 | 16 | 53 | 30 | 54 | 7 | 6 | 6 | 2 | 0 | 54 | 13 | 7 | 5 | 0 |
| 8 | 40 | 25 | 30 | 30 | 8 | 5 | 15 | 0 | 1 | 55 | 9 | 3 | 6 | 3 |
| 9 | 45 | 9 | 19 | 26 | 9 | 7 | 2 | 3 | 6 | 56 | 5 | 3 | 6 | 4 |
| 10 | 30 | 37 | 5 | 13 | 10 | 4 | 5 | 2 | 9 | 57 | 5 | 3 | 6 | 0 |
| 11 | 24 | 37 | 33 | 31 | 11 | 6 | 12 | 8 | 14 | 58 | 3 | 0 | 2 | 5 |
| 12 | 39 | 29 | 17 | 44 | 12 | 2 | 9 | 12 | 12 | 59 | 12 | 7 | 2 | 12 |
| 13 | 22 | 17 | 35 | 26 | 13 | 4 | 19 | 4 | 14 | 60 | 10 | 7 | 5 | 9 |
| 14 | 26 | 29 | 40 | 52 | 14 | 3 | 14 | 9 | 10 | 61 | 7 | 8 | 3 | 3 |
| 15 | 33 | 19 | 19 | 18 | 15 | 3 | 5 | 7 | 10 | 62 | 9 | 8 | 9 | 5 |
| 16 | 40 | 38 | 28 | 8 | 16 | 17 | 7 | 4 | 3 | 63 | 9 | 2 | 6 | 0 |
| 17 | 21 | 33 | 39 | 26 | 17 | 12 | 2 | 1 | 6 | 64 | 6 | 7 | 13 | 6 |
| 18 | 17 | 27 | 28 | 51 | 18 | 16 | 6 | 0 | 0 | 65 | 6 | 10 | 4 | 4 |
| 19 | 35 | 15 | 35 | 22 | 19 | 8 | 13 | 3 | 6 | 66 | 12 | 2 | 11 | 11 |
| 20 | 17 | 30 | 17 | 22 | 20 | 10 | 11 | 8 | 16 | 67 | 9 | 9 | 9 | 5 |
| 21 | 14 | 38 | 41 | 28 | 21 | 12 | 12 | 11 | 9 | 68 | – | 19 | 1 | 5 |
| 22 | 28 | 32 | 15 | 13 | 22 | 8 | 4 | 4 | 18 | 69 | – | 3 | 5 | 9 |
| 23 | 22 | 21 | 42 | 9 | 23 | 5 | 4 | 6 | 8 | 70 | – | 8 | 5 | 10 |
| 24 | 21 | 27 | 26 | 5 | 24 | 10 | 7 | 12 | 0 | 71 | – | 9 | 4 | 14 |
| 25 | 24 | 27 | 20 | 29 | 25 | 9 | 2 | 6 | 6 | 72 | – | 5 | 5 | 10 |
| 26 | 28 | 26 | 12 | 25 | 26 | 1 | 5 | 13 | 18 | 73 | – | 7 | 8 | 13 |
| 27 | 29 | 30 | 21 | 5 | 27 | 11 | 1 | 5 | 7 | 74 | – | 10 | 13 | 7 |
| 28 | 27 | 28 | 17 | 15 | 28 | 3 | 5 | 7 | 5 | 75 | – | 15 | 15 | 8 |
| 29 | 23 | 12 | 20 | 6 | 29 | 6 | 5 | 1 | 2 | 76 | – | 8 | 14 | 15 |
| 30 | 42 | 27 | 22 | 35 | 30 | 8 | 16 | 4 | 3 | 77 | – | 5 | 7 | 4 |
| 31 | 29 | 29 | 14 | 26 | 31 | 14 | 5 | 10 | 0 | 78 | – | 5 | 11 | 6 |
| 32 | 27 | 12 | 30 | 9 | 32 | 10 | 7 | 19 | 10 | 79 | – | 7 | 8 | 1 |
| 33 | 42 | 23 | 43 | 34 | 33 | 4 | 8 | 1 | 8 | 80 | – | 2 | 13 | 5 |
| 34 | – | 36 | 35 | 20 | 34 | 4 | 4 | 10 | 13 | 81 | – | – | 10 | 6 |
| 35 | – | 24 | 17 | 24 | 35 | 5 | 7 | 7 | 18 | 82 | – | – | 6 | 10 |
| 36 | – | 42 | 19 | 36 | 36 | 5 | 5 | 6 | 0 | 83 | – | – | 6 | 3 |
| 37 | – | 31 | 32 | 50 | 37 | 6 | 3 | 7 | 5 | 84 | – | – | 4 | 5 |
| 38 | – | 38 | 41 | 45 | 38 | 7 | 5 | 0 | 8 | 85 | – | – | 8 | 14 |
| 39 | – | 29 | 43 | 25 | 39 | 3 | 6 | 5 | 2 | 86 | – | – | 5 | 11 |
| 40 | – | 17 | 38 | 21 | 40 | 1 | 10 | 8 | 3 | 87 | – | – | – | 7 |
| 41 | – | – | 43 | 15 | 41 | 6 | 18 | 10 | 10 | 88 | – | – | – | 15 |
| 42 | – | – | 40 | 33 | 42 | 6 | 9 | 3 | 0 | 89 | – | – | – | 22 |
| 43 | – | – | 23 | 18 | 43 | 7 | 7 | 0 | 10 | 90 | – | – | – | 13 |
| 44 | – | – | – | 36 | 44 | 9 | 9 | 10 | 0 | 91 | – | – | – | 17 |
| 45 | – | – | – | 36 | 45 | 5 | 3 | 4 | 9 | 92 | – | – | – | 13 |
| 46 | – | – | – | 55 | 46 | 2 | 9 | 7 | 3 | 93 | – | – | – | 5 |
| 47 | – | – | – | 53 | 47 | 4 | 6 | 11 | 0 | – | – | – | – | – |
| n | 33 | 40 | 43 | 47 | | 67 | 80 | 81 | 88 | | | | | |
| avg | 27.5 | 27.2 | 26.3 | 26.1 | | 6.7 | 7.0 | 6.3 | 6.6 | | | | | |
| std | 8.6 | 9.6 | 11 | 14 | | 3.5 | 4.3 | 4.1 | 4.9 | | | | | |

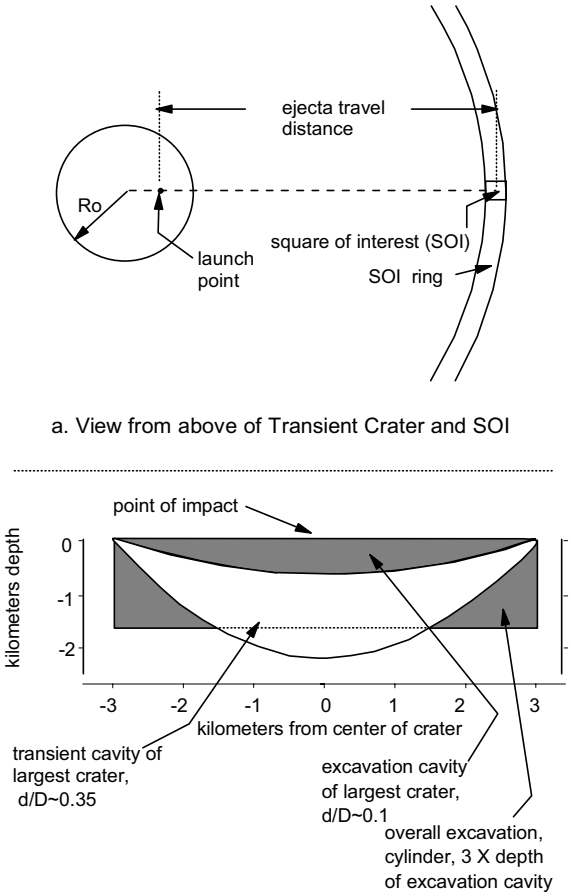


Fig. 3. a) The relationships between the primary crater, the launch point, and the ejecta travel distance to the SOI are shown; b) A cross section through the center of the paraboloid of revolution with depth/diameter of 0.10 used for the excavation cavity of secondary craters is shown to scale. The quantity of substrate excavated corresponds to that of a cylinder with the diameter of the paraboloid excavation cavity produced by the largest PriFrag to strike that location and a height equal to ~3 times its depth. All PriFrags landing within the circumference of that paraboloid and their excavation products are incorporated into the mixture that becomes the ejecta deposit.

realism of our model is discussed later in the paper. Some concepts used in the modeling are illustrated in Fig. 3.

### Step 1. Selecting a Square of Interest (SOI)

The first step in the model is to define the size and location of the "square of interest" (SOI). For basin-sized events, we use a 100 × 100 km square centered on the site of interest. The SOI is a 100 km long segment within the 100 km wide circumferential ring lying at the distance of interest from the center of the primary crater (Fig. 3a). A 100 × 100 km square would encompass most proposed rover traverses and could have a substantial range of ejecta deposit properties. This size can be scaled down for smaller primary craters of interest.

Table 2. Nominal values used for modeling.

| |
|---|
| PriFrag size distr. (Equation 1) |
| b = 0.85 |
| max PriFrag size (Equation 5) |
| coeff = 0.05 |
| expon = 0.8 |
| max PriFrag size cutoff (Equation 5) |
| $V_{min}$: depends on crater size |
| c = –2.0 |
| Housen et al. eqn. (Equation 7) |
| A = 0.2 |
| $e_x$ = 1.81 |
| $e_r$ = 2.83 |
| θ = 45° |
| Secondary craters (Equations 10 and 11) |
| d/D transient = 0.35 |
| d/D excavation = 0.1 |
| α = 0.65 |
| $A_g$ = 0.2 |
| β = 0.83 |
| $A_s$ = .49 |
| Y = 10 Mpa |
| Excavation depth (Equation 14) |
| DM = 3.0 |

### Step 2. Calculating the Mass Distribution

We use the following power law, based on measurements of primary fragment (PriFrag) sizes from laboratory craters, explosion craters, and terrestrial impact craters (Hartmann 1969; Melosh 1989; Turcotte 1992) to obtain the cumulative PriFrag size distribution:

$$N(\geq m) = Cm^{-b} \quad (1)$$

In Equation 1, N(≥m) is the total number of PriFrags with mass greater than or equal to m, C is a constant, and b is the fragmentation exponent. Equation 1 implies an incremental distribution that can be convolved with m to yield a total ejected mass

$$M_T = C\frac{b}{b-1}(m_h^{1-b} - m_l^{1-b}) \quad (2)$$

where $m_h$ and $m_l$ are upper and lower limits of integration. We arbitrarily start calculations at 0.1 gram as the smallest PriFrag mass. Studies of rock fragmentation by laboratory experiments and explosions indicate that the value of b is between 0.8 and 0.9 (Melosh 1989; Turcotte 1992), such that most of the mass is carried by the larger PriFrags (blocky ejecta). Some remote sensing studies of the Moon suggest, however, that b > 1 for crater ejecta (e.g., Shoemaker 1965). This may be a consequence of increased comminution during the secondary cratering process (Schultz and Mendell 1978). We chose a value of b = 0.85 for most of the modeling.

In practice, we divide our mass range into small mass

increments, $\Delta m = m_x - m_y$, to obtain $\Delta N$, the number of PriFrags within that mass increment.

$$N(\geq m_x) - N(\geq m_y) = \Delta N \quad (3)$$

The mass of the individual PriFrags within each interval ($m_{avg,\,i}$) is closely approximated by the average of $m_{i-1}$ and $m_i$ as long as the interval is small, so that

$$M_i = (\Delta N)(m_{avg,\,i}) \quad (4)$$

A constraint on the upper limit of mass of the largest fragment in the distribution has been suggested by O'Keefe and Ahrens (1987) and is based on observations of terrestrial craters (Gault, Shoemaker, and Moore 1963; see also Moore 1971). They propose that the mass ($M_f$) of the largest fragment produced during an impact event is given by:

$$M_f = 0.05 M_T^{0.8} \quad (5)$$

where both $M_f$ and $M_T$ are in kilograms. We use this constraint for the largest PriFrag size bin for our modeling. O'Keefe and Ahrens (1987) also indicate that the maximum PriFrag size should decrease with ejection velocity. We therefore modify the value given by Equation 5 by their factor $(V/V_{min})^c$, where c is an empirically determined constant. O'Keefe and Ahrens give a value for c of –3. Cintala, Garvin, and Wetzel (1982) found a somewhat steeper exponent of –3.7 from block counts around a lunar crater. The average value determined by Vickery (1987) for secondary craters around several lunar craters is $c = -2.1 \pm 0.6$. The minimum velocity ($V_{min}$) as defined by O'Keefe and Ahrens (1987, their Equation 7) is the minimum velocity of ejection of solid particles. The choice of a minimum ejecta velocity $V_{min}$ appears to be somewhat arbitrary, however, and it is difficult to know what value should be assigned. In applying the equation to her study of the sizes of ejected blocks, Vickery (1986) chose the velocity required to move a block from the edge of the transient crater to the rim of the present crater as the minimum velocity. This choice for $V_{min}$ is not obviously applicable to the Imbrium situation we are modeling here, but we take it as a starting point. For Imbrium, the velocity required to lift a PriFrag from the position of the edge of the transient crater to the position of the edge of the final crater is ~0.53 km/s. For most of the modeling, we used a $V_{min}$ of 0.53 km/s and c = –2.0, giving greater weight to observations of lunar secondary craters.

The sum of the masses over all the intervals of distance must equal the total mass ($M_T$) ejected from the primary crater (equivalent to determining C in Equation 1). We estimate $M_T$ in Equation 6 by assuming an excavation cavity of the primary crater that is parabolic with a transient crater radius $R_0$ and with a depth to diameter ratio of 1:10 (Melosh 1989, p. 78), but with 10% of the volume of the paraboloid excluded to account for material not ejected, as in a Z model (mostly, material under the impact point; Melosh's Fig. 5.13).

$$M_T = 0.09 \rho \pi R_0^3 \quad (6)$$

We use a target density ρ of 3 g/cm$^3$. We observe that the scaling laws for primary excavation craters appear to be accurate even for basin-sized events. A supportive recent test comes from the work of Wieczorek and Phillips (1999), who used elevation and gravity data to determine the shapes and volumes of excavation cavities for several basins. They assumed a two-layer crustal model and that the mascon character of the basins was mainly a consequence of mantle rebound. By suppressing the Moho under each basin to its presumed pre-basin depth, they obtained excavation cavity shapes that are roughly parabolic and, for all except three of the basins tested, they obtained an average depth/diameter of 0.11, essentially identical to the value of 0.10 determined for appropriate impact cavities many orders of magnitude smaller (though, see later discussion). They obtained lower values of depth/diameter for the Imbrium, Serenitatis, and South Pole-Aitken basins. One of the explanations they offer for the shallower depths of the Imbrium and Serenitatis basins is viscous relaxation. This is plausible in that the Procellarum KREEP Terrane that contains the Imbrium basin and borders the Serenitatis basin and perhaps extends across it (Jolliff et al. 2000) was presumably still hot when those basins formed (see also Haskin 1998; Haskin et al. 1998). If we accept this explanation for the Imbrium and Serenitatis basins, then the quantity and average radial distribution of ejecta is indeed that expected from the scaling relationships, and we thus regard the predicted mass of PriFrags to be a robust tenet of the modeling. We ignore the South Pole-Aitken basin in this work because it is recognized to be generally anomalous (e.g., Spudis, Reisse, and Gillis 1994; Schultz 1998).

### Step 3. Calculating the Mass of Primary Ejecta at a Specific Location

The equations for ejecta scaling are given for a flat surface (e.g., Housen, Schmitt, and Holsapple 1983), but the sphericity of the Moon is important to the properties of basin-produced ejecta deposits. We map the results for a flat body onto a spherical one, using velocity as the controlling parameter because the velocity of the infalling PriFrags determines distance and excavation efficiency. We use Equation 7 (Housen, Schmitt, and Hosapple 1983, for a flat target in a constant gravity regime) to calculate the thickness of the hypothetical average layer of PriFrags landing on an SOI, then convert the thickness into a mass by using the assumed density (ρ ~3 g/cm$^3$).

$$\frac{t}{R_0} = \frac{A(e_r - 2)}{2\pi}(\sin 2\theta)^{e_r - 2}\left(\frac{R}{R_0}\right)^{-e_r} \times \left[1 + \frac{4e_r - 5}{3}\left(\frac{R/R_0}{\sin 2\theta}\right)^{-(e_r - 2)/2}\frac{0.62^{1/e_x}}{R/R_0}\right] \quad (7)$$

Here, $t/R_0$ is the thickness normalized to the apparent (the ground plane, or transient) crater radius, R is the distance from the center of the crater, A is an empirical constant (equal to ~0.20 in the gravity regime based on impact experiments in sand by Stöffler et al. (1975), as analyzed by Housen, Schmitt, and Hosapple (1983), their Fig. 6), θ is the launch angle relative to the surface, and $e_r$ and $e_x$ are crater scaling exponents. In the far-field limit, where most of the attention in this paper is paid, the change in thickness with distance from the primary crater is mainly dependent on $(R/R_0)^{-e_r}$ (the term in brackets goes to one); we adopt zero-porosity, gravity-regime values $e_r = 2.83$ and $e_x = 1.81$ from Housen, Schmitt, and Hosapple (1983), which are the most appropriate for basin-scale events. Literature information on launch angles varies widely. We use 45° as our nominal value, which is supported by the recent measurements of Cintala, Berthoud, and Hörz (1999), cf. later discussion.

Over what distance range might we expect this scaling relationship to hold? It was developed primarily from laboratory studies, with confirmation from explosion ejecta on a larger scale and to the extent possible from observations of large impact craters. Based on the laboratory data of Andrews (1975; see, e.g., Fig. 8 of Housen, Schmitt, and Hosapple 1983), the scaling relationship holds from ~2 transient crater radii out to a distance of some 15–20 transient crater radii (flat surface). For scale, the ejecta velocity to reach the lunar antipode is the same as that required to reach a distance of ~9 transient crater radii from the center of an Imbrium-sized basin on a flat surface, well within the laboratory tested distance.

For our modeling, we regard the lunar surface as a set of successive 100 km wide rings of SOIs lying radially outward from the transient crater (Fig. 3). Equation 7 was derived by Housen, Schmitt, and Hosapple (1983) from scaling laws for the velocity of ejecta as a function of position within the growing crater. Specifically, it was derived assuming the launch position is a small, but non-negligible, fraction of the distance the ejecta travel, $R_s$. We assume, for simplicity, that the PriFrag launch site is at half the transient radius, $R_0/2$ (as in Morrison and Oberbeck 1978). Thus, for any ejecta range on the Moon, $R_e$, $R_s = R_e - R_0/2$, and the launch velocity given by the range-velocity equation for a spherical surface (e.g., Melosh 1989, p. 87) is:

$$U = \frac{\sqrt{R_m g \tan X}}{\sqrt{\tan X \cos\theta^2 + \sin\theta\cos\theta}} \quad (8)$$

where $R_m$ and g are the radius and surface gravity and X is the ratio defined by $(R_s/2R_m)$, where $R_s$ is the arc distance from the launch point (here, to the center of the SOI). The distance PriFrags travel on a flat surface for that launch velocity is obtained from the range-velocity equation for a flat surface. This launch velocity corresponds to a range on a flat target of

$$R = R_0/2 + U^2 \sin\theta/g \quad (9)$$

which can be used in Equation 7 to determine the thickness of ejecta falling on an SOI. Note that equally spaced SOIs on the Moon will correspond to unequally spaced SOIs on the flat target.

**Step 4. Calculating the Incremental Number of PriFrags per SOI**

From the average thickness of the PriFrag layer (Step 3) on the SOI and the mass distribution and choice of $M_f$ (Step 2), we calculate the mass and the number of PriFrags in each size range falling on the SOI. The number of PriFrags in any size or mass range is in general not an integer.

**Step 5. Determining Secondary Crater Sizes**

The size of the secondary crater produced by a PriFrag depends on the PriFrag mass, ejection angle, and velocity. We obtain the diameters of the secondary craters from the π scaling relationships described by Holsapple and Schmidt (1982), Schmidt and Housen (1987), and Holsapple (1993). A parabolic *transient* secondary crater is assumed with a d/D of 0.35 (e.g., Melosh 1989, p. 144), from which we obtain the diameter of the crater. Fig. 3 of Holsapple (1993) illustrates the relationships shown in Equations 10 and 11 for cratering efficiency, $\pi_v$, defined as the ratio of the "mass of material of the crater" (i.e., the volume of the transient crater times the density of the material that was in the transient crater volume) to the mass of the impactor. The variables in Equations 10 and 11 are velocity (U), density (δ) of the PriFrag, gravity (g), and substrate material strength (Y). For a crater that forms in the gravity regime,

$$\pi_v = A_g\left(\frac{1.61 g d}{U^2}\right)^{-\alpha} (\sin\theta)^{2\alpha} \quad (10)$$

where $A_g$ and α are experimentally derived constants, d is the diameter of the (spherical) projectile striking the target, and θ is the angle of impact with respect to the horizontal (equal to the launch angle, here 45°). For secondary craters that form in the strength regime, (e.g., in competent basalt flows,) and assuming strengths that are neither scale nor rate dependent,

$$\pi_v = A_s\left(\frac{Y}{\delta U^2}\right)^{-\beta} (\sin\theta)^{2\beta} \quad (11)$$

where $A_s$ and β are constants derived from experimental data. The experimentally derived exponents α and β are theoretically related to each other by $\beta = 3\alpha/(3-\alpha)$ (e.g., Holsapple and Schmitt 1982). We assume that Y = ~10 MPa (close to the value of Y = 7 MPa from Holsapple [1993; his Fig. 7 for hard rock]). The impact angle dependence is taken from Chapman and McKinnon (1986).

**Step 6. Determining Cumulative Total Area Covered with Craters of Each Diameter**

By combining the results of Steps 4 and 5, we know the number of secondary craters produced by PriFrags of each mass interval per SOI. This allows us to calculate the percentage of the SOI covered by secondary craters of a given diameter. Using a Poisson distribution, Garwood (1947) presented a relationship for random circles (bombs) falling on a rectangular surface:

$$W = 1 - e^{-\lambda K} \quad (12)$$

Here, W is the fraction of the surface of the SOI that is "saturated," i.e., the fraction that has been excavated by the secondary craters, λ is the area excavated by an impacting PriFrag of a given size (which we take as the area of the paraboloid of excavation of the secondary crater), and K is the number of PriFrags of that size that strike per unit area of the surface. In a particular calculation, K is usually not an integer. Equation 12 can be applied to PriFrags in each size range. The cumulative total fraction of area covered by PriFrags in all the SOI mass increments ($W_T$) is then:

$$W_T = \sum_{i=1}^{n} (W_i - W_i W_{i-1}) \quad (13)$$

where n is the number of increments used and $W_i$ is the fraction of the area saturated by PriFrags in each mass increment.

**Step 7: Calculating the Excavation Efficiency**

The thickness of an ejecta deposit depends on the surface density of PriFrags and on the depth to which the PriFrags excavate. The former comes from Equation 7; the latter requires knowledge of the excavation efficiency. Oberbeck et al. (1975) formulated a "cratering efficiency" μ, defined as the ratio of the mass of the material *excavated* from a secondary crater to the mass of the PriFrag that produced that crater. Their formulation is based on the ballistic equation and on empirical explosion data and the size of craters produced. Note that this definition of cratering efficiency is not the same as that of $\pi_v$ given by Holsapple (1993; Equations 10 and 11 above), which is based on the volume of the transient crater. Here, we will use the term "excavation efficiency" for the ratio of the mass of material excavated from a crater to the mass of the PriFrags producing the crater and will represent it by μ. For the modeling done here, the excavation cavity is presumed equivalent in volume to a paraboloid with the same diameter as the transient cavity, but a lower depth/diameter ratio of 0.1.

We define an *individual PriFrag μ value*, $\mu_{indiv}$, for a secondary crater produced by a single PriFrag, as the ratio of the mass of the material ejected from the secondary crater to the mass of that PriFrag. This $\mu_{indiv}$ value is comparable in concept to the μ of Oberbeck et al. (1975, their Equation A3, Appendix A) and Morrison and Oberbeck (1978), which we will refer to as $\mu_{Ober}$. The values obtained from their formulation can differ substantially from ours, however. For example, at the Apollo 16 site, impact angle of 45°, for 1 km PriFrags, $\mu_{indiv}$ = 2.1 and $\mu_{Ober}$ = 11.5; for the far more numerous 10 m PriFrags, $\mu_{indiv}$ = 42 and $\mu_{Ober}$ = 49. The differences occur for at least three reasons: 1) Oberbeck et al. used different (earlier) scaling equations; 2) they assumed an excavation depth equal to the full transient crater depth, with a depth/diameter of 0.25; and 3) they assumed a much shallower ejecta angle of ~15° to the horizontal.

We cannot apply $\mu_{Ober}$ or $\mu_{indiv}$ to each PriFrag striking the SOI as if it struck undisturbed substrate. Many PriFrags affect the same location of an SOI almost simultaneously. Also, for small PriFrags, cratering efficiencies calculated by $\mu_{Ober}$ or $\mu_{indiv}$ are large and, if applied cumulatively to fresh substrate, lead to exaggerated depths of excavation. To obtain a geologically more realistic μ, we begin with a geometric estimate based on the parabolic excavation crater produced by the largest PriFrag excavating at a given spot within an SOI. Other smaller PriFrags impacting within that cavity are presumed partly to mix with substrate that is excavated by the largest PriFrag, and partly to excavate additional substrate. As a starting point, we estimated the total mass of substrate excavated from the crater produced by the largest PriFrag excavating the spot in question as the mass contained in a cylinder with the diameter and depth of the parabolic excavation cavity produced by that largest PriFrag. The ratio of this mass to the combined masses of *all* the PriFrags falling within the excavation cavity of the largest PriFrag was thus our *initial* estimate of μ, $\mu_{init}$.

To better estimate the amount of substrate excavated by these smaller PriFrags, we introduce an empirical constant, the "depth multiplier" DM, and obtain our *effective* μ ($\mu_{eff}$) by calibrating to two sets of data on deposit thicknesses from the literature (discussed below). The outcome of the calibration is that DM ~3. The volume excavated at any specific location within an SOI is thus the cylinder described by Equation 14, in which $D_{LPF}$ is the diameter of the largest secondary crater containing that location, and $d_{LPF}$ is the depth of that crater.

$$V_{excav} = \pi \times (D_{LPF}/2)^2 \times d_{LPF} \times DM \quad (14)$$

That is, the smaller PriFrags, along with the largest PriFrag, excavate a cylinder some three times deeper than the excavation cavity of the largest PriFrag. In this formulation, ~17% of the substrate is excavated by the largest PriFrag, and the remaining 83% is excavated by the rest of the PriFrags that fall within the crater (though the actual time sequence is indeterminate). The excavation cavity of the largest PriFrag, the transient crater, and the cylinder of excavation are shown to scale in Fig. 3b. The number of smaller PriFrags of each size range that fall within the area excavated by the larger

PriFrags is taken to be the number that would fall randomly onto that area. Dividing the excavated mass by the sum of the masses of all the PriFrags striking the location gives us $\mu_{eff}$, which we use in our modeling.

$$\mu_{eff} = \mu_{init} \times DM \quad (15)$$

For comparison with the values of $\mu_{indiv}$ and $\mu_{Ober}$ given above, at the Apollo 16 site, $\mu_{eff} = 4.8$ for secondary craters produced by a largest PriFrag of 1 km diameter, and $\mu_{eff} = 4.4$ for those produced by a largest PriFrag of 10 m diameter.

This means of envisioning the process of excavation should not be taken as a literal physical model. When ballistic sedimentation takes place, the largest PriFrag to excavate at a particular location may dominate to an extent, but it does not necessarily arrive first, with its excavation cavity then reamed out by later-arriving, smaller PriFrags, although the model we used to obtain our $\mu_{init}$ value might seem to imply such a sequence. Rather, the model leading to $\mu_{init}$ is just a conceptual means of obtaining a depth of excavation that might be reached by the scouring action of the PriFrags acting at a given location within the SOI, a depth easily corrected by empirical information. The mutual action of so many PriFrags arriving almost simultaneously provides a surge of excavation, mixing, and bulk radial flow that would be difficult to model without resorting to direct numerical simulation.

Schultz and Gault (1985) describe a clustered impact model for secondary craters and provide experimental results in which material of a given mass in the form of a group of impactors, rather than as a single impactor, strikes a target. They regard their results as providing a better description of secondary crater formation than a single impactor model. The morphology of some of their experimental craters is consistent with mutual interference by ejecta from several or many impactors arriving simultaneously at the target. The $\mu$ value derived from their results is only 0.1 to 0.5 times the $\mu$ value from single impactors of comparable mass. Qualitatively, their results are consistent with ours, in that $\mu_{eff}$ is lower than $\mu_{init}$ in most instances, but quantitative comparison is not possible.

Our modeling does not explicity take into account the horizontal momentum of the fallen PriFrags (Oberbeck 1975) or the locations of the secondary ejecta that surround each excavation. We assume that material carried out of an SOI by radial momentum is replaced by a similar or greater quantity of material from the adjacent SOI. This is reflected in our empirical DM value, which accounts for effects of churning and stripping of the lunar surface by the ejecta surge.

### Variations in Deposit Thickness and %PriFrags within an SOI; Coverage Level

Because different locations within the SOI have been excavated by largest PriFrags of different sizes, there is a distribution of excavation depths, deposit thicknesses, and values of $\mu_{eff}$ over the area of the SOI. The actual locations within the SOI of the excavations of different sizes are random and are thus not predicted by the model. The fraction of the area covered by circles of excavation produced by PriFrags of a particular size increment is given by Equation 12. PriFrags of each successively smaller size increment excavate some territory not already excavated by PriFrags of the next larger size. This trend continues to the point that the PriFrags of a particular, relatively small size are so numerous that they excavate the entire SOI, as will PriFrags of even smaller sizes.

To illustrate the variation in ejecta deposit properties expected within an SOI, we define a term "coverage level" as the total fraction of the SOI that has been excavated by craters of a particular diameter and larger. Coverage level refers only to the fraction of the total SOI area that has been *excavated*, and does not include areas covered by secondary crater ejecta. It would be equivalent to report coverage level as the fraction of the SOI that has been excavated by PriFrags of a given size increment and larger, because crater diameter depends directly on PriFrag size and velocity. Note, however, that *coverage level is specific to an SOI and primary crater and is not constant for a particular size of PriFrag or size of crater.* Coverage level depends on the surface density of PriFrags of every diameter that reach the SOI and on PriFrag velocity and is thus specific to a given ring of SOIs surrounding a given primary crater. It would further be equivalent to report coverage level in terms of depth of excavation or deposit thickness, as these quantities also correlate with PriFrag size for a given SOI. For example, if the coverage level associated with PriFrags in increment a is 30% of the SOI (CL30%), then 30% of the SOI has been excavated by craters as large as or larger than those produced by PriFrags of increment a, and the excavations are as deep as or deeper than the maximum depth reached by PriFrags of increment a times the depth multiplier DM (see Equations 14 and 15).

## RESULTS OF MODELING

### Relationships among Primary Crater Size, Thickness of Ejecta Deposit, Fraction of PriFrags in the Ejecta Deposit, and Distance of the SOI from the Primary Impact Site

Nominal values of model parameters used in this paper, i.e., those values used unless otherwise stated, are given in Table 2. Some general characteristics of *average* ejecta deposits can be seen in Fig. 4, where thicknesses of the deposits and %PriFrags in the deposits are shown as functions of distance from the center of a primary crater, in this case, Imbrium (see also Haskin 1998). The transient radius of the Imbrium crater is taken to be 370 km (Wieczorek and Phillips 1999).

The dependence of ejecta deposit thickness on distance

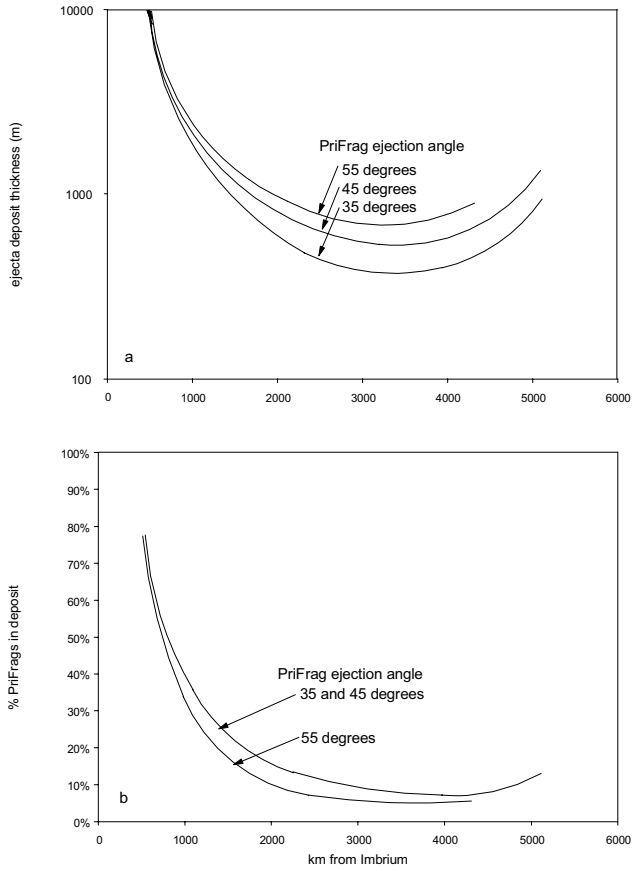


Fig. 4. The modeled thicknesses of ejecta deposits from the Imbrium event and the proportion of Imbrium ejecta in the deposits are shown for three ejection angles as a function of distance from the Imbrium basin. The values shown are for CL50% (see text for definition). No estimates are shown close to the Imbrium antipode, where the rotation of the Moon can affect their location. The curve for 55° ends at ~4300 km because ejecta with higher velocities are lost from the Moon.

from the primary crater is shown in Fig. 4a. These results are for a 50% coverage level (CL50%). The principal feature is a decrease in deposit thickness with increasing distance from Imbrium, passage through a minimum, then an increase. The initial decrease occurs because the amount of ejecta (and thus the surface density) decreases rapidly with distance from the point of primary impact. A broad minimum occurs at ~3100 to 3500 km. The increase beyond the minimum occurs for two reasons: 1) The circumference of the ring of SOIs decreases past the halfway point to the antipode (2730 km), so the surface density of PriFrags increases from the minimum value despite the decrease in total PriFrag mass with increasing distance from the primary crater; 2) The higher velocity ejecta that reach greater distances from the primary crater are more efficient excavators than their lower velocity counterparts (Equation 10). Special effects on deposit thickness are expected in the vicinity of the antipode (5460 km) because of long flight times and the rotation of the Moon, so the calculations are not carried out to that distance (e.g., Dovrobolskis 1981; Haskin, McKinnon, and Benner 1996; Wieczorek and Zuber 2001). If the ejection angle θ is steep (e.g., 55°), ejecta with higher velocities cannot approach the antipode but are lost from the Moon. Note that the mass ejected to the far field is not as conserved as θ is varied; mass balance is presumably achieved in the near field, where Equation 7 breaks down.

The dependence of the fraction of PriFrags in the ejecta deposits (%PriFrags) on distance from Imbrium is shown in Fig. 4b. Near the Imbrium basin, the ejecta have relatively low velocity, so they excavate with only modest efficiency, and the surface density of large PriFrags is high enough to saturate the SOIs. The remaining PriFrags also have low velocity, so the proportion of PriFrags in the deposits is high. Downrange, as the velocity increases and the surface density of PriFrags decreases, the proportion of PriFrags in the deposits decreases. Finally, the circumference of the SOI ring shrinks sufficiently that despite the falloff in the amount of PriFrags with distance from the primary crater, the surface density of PriFrags increases to the extent that the %PriFrags in the deposits again increases. The broad minimum in the curve occurs at ~3500 to 3900 km, well past the halfway point to the antipode and past the minimum in deposit thickness. Note that the %PriFrags is not strongly sensitive to the ejection angle.

Results of modeling of the Imbrium ejecta deposits are shown in Fig. 5 for CL20%, CL50%, and CL80% at a single distance from the center of Imbrium, namely, the SOI ring at ~1600 km that contains the Apollo 16 landing site. The depth of excavation (not shown) and the deposit thickness decrease sharply with increasing coverage level (smaller PriFrags produce smaller but more numerous craters than larger PriFrags produce, so craters of smaller diameters yield higher coverage levels).

For the model results illustrated in Fig. 5a, at 1600 km from Imbrium and a 45° ejection angle, some additional observations are that the radii of largest PriFrags excavating the deepest 20% of the SOI are 860 m and larger, those excavating the deepest 50% are 460 m and larger, and those excavating the deepest 80% are 230 m and larger. The resulting secondary craters have diameters of 4.8 km and larger, 2.9 km and larger, and 1.7 km and larger. Some 90 largest PriFrags excavate the deepest 20% of the SOI, 600 largest PriFrags excavate the deepest 50%, and 3200 largest PriFrags excavate the deepest 80% of the SOI. Actual deposit thicknesses are expected to deviate from the averages shown here, because the ejection of PriFrags is expected to be more or less azimuthally stochastic.

The minimum size of largest PriFrag that (along with larger PriFrags) excavates at a given coverage level decreases with distance from the primary crater mainly because the surface density of PriFrags of all sizes decreases with distance. That is, PriFrags of the sizes that excavate to CL50% at a range of 1000 km (PriFrags 950 m and larger,

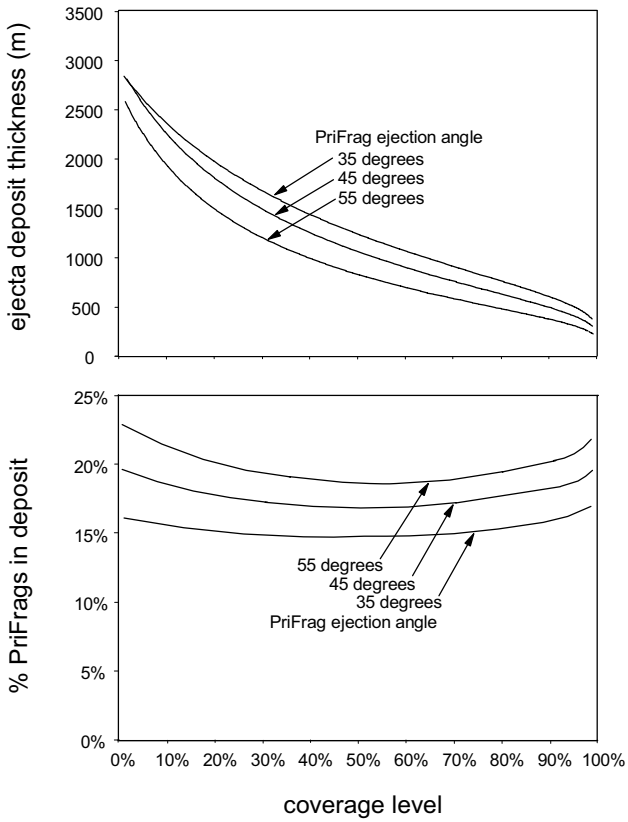


Fig. 5. The modeled variation in thicknesses of ejecta deposits from the Imbrium event at a specific location is shown for three ejection angles as a function of coverage level. The percent of primary ejecta (PriFrags) in the deposits is nearly constant with coverage level in this case. This case is for 1600 km from Imbrium, the distance of the Apollo 16 landing site.

craters 4.7 km and larger) are too scattered to excavate such a high fraction of an SOI at a range of 1600 km (only CL17% there, although the craters produced are slightly larger). At great enough distances, the ejecta converge on the side of the Moon opposite the primary crater, and with the resulting increase in PriFrag surface density, the PriFrags that excavate to CL50% are again larger.

Although the thickness of the deposits at 1600 km varies substantially as a function of coverage level, the fraction of PriFrags in the deposits does not, ranging only between 17% and 20% over the entire range (45° launch angle). The mixture of materials from different provenances is thus about the same whether samples are taken from a site within the SOI where the deposit is relatively thick or relatively thin. This is a typical result of the modeling, that %PriFrags usually does not vary much with deposit thickness within an SOI.

In way of comparison with other modeling, Morrison and Oberbeck (1975) estimated that the Apollo 16 smooth plains deposits contain not more than 13–18% Imbrium material. Our estimates do not always match theirs, however. We estimate 31–33% PriFrags in the Fra Mauro deposits at Apollo 14, significantly higher than the estimate of 15–20% Imbrium ejecta by Morrison and Oberbeck (1975) and implying that Imbrium ejecta would be more common at that site than previously estimated.

**Potential Consequences of the Modeling for Sampling and Provenance; The Apollo 16 Site**

Our modeling is an effort to account for the large quantities of material excavated from a basin, interaction of that ejected material with a target substrate (at a given distance from the basin center), and the average gross features of the ejecta deposit that is produced. Based on this modeling, we can consider the development of the stratigraphy of basin deposits at the Apollo 16 landing site as follows: Starting with a pre-Nectarian substrate (mainly pre-Nectarian megaregolith deposits, possible in situ igneous formations, etc.), the order of formation of the basins considered here is Nectaris, Humorum, Crisium, Serenitatis, Imbrium, and Orientale (Wilhelms 1987). Given the standard parameters of Table 2 and a radius of 208 km for the Nectaris transient crater (Wieczorek and Phillips 1999), the modeling suggests that the original (pre-Serenitatis) Nectaris deposit at the distance of the Apollo 16 site ranged in thickness (CL10% to CL90%) from ~1.9 to 0.6 km and contained ~33% Nectaris PriFrags, with the rest of the deposit consisting of pre-Nectarian substrate. (Note that deposit thicknesses in Haskin et al. (2002) were based on $\mu_{init}$ rather than $\mu_{eff}$ and are, therefore, lower and with %PriFrags greater than the estimates given in this work.)

The Humorum and Crisium events produced only shallow deposits at the Apollo 16 site and did not excavate deep into the Nectaris deposit. Again based on the standard parameters and a radius of 327 km for the Serenitatis transient crater (Wieczorek and Phillips 1999), Serenitatis PriFrags excavated to depths ranging from ~1.8 to 0.5 km, through even the thickest parts of the Humorum and Crisium deposits. Depending on the relative locations of the deeper excavations by Serenitatis PriFrags and the shallower regions of the Nectaris deposits, at some locations, Serenitatis PriFrags could have excavated through the entire Nectaris deposit, as well. The model predicts that the original (pre-Imbrium) Serenitatis deposit at the distance of the Apollo 16 site ranged in thickness (CL10% to CL90%) from ~2.5 to 0.7 km and contains ~25% Serenitatis PriFrags.

As described above, the Imbrium deposit ranges in thickness (CL10% to CL90%) from ~2.2 to 0.5 km and contains ~18% Imbrium PriFrags. The Imbrium PriFrags mainly excavated to depths ranging from ~1.8 to 0.4 km, and depending on the relative locations of the deeper excavations by Imbrium PriFrags and the shallower regions of the Serenitatis deposits, the Imbrium deposit presumably excavated through the entire Serenitatis deposit at some locations. Thus, in such locations, the Imbrium deposit would

be in direct contact with part of the Nectaris deposit.

Based on the modeling, the last formed basin deposit, the one produced by the Orientale event, can be ignored. Its thickness ranged only from 0.4 to 0.05 km and it contained only ~2% Orientale PriFrags, with the rest of the material coming from the upper part of the thick Imbrium deposit. That deposit has presumably been gardened into the underlying Imbrium deposit by smaller cratering events with little consequence to the provenance composition of the Imbrium deposit. Post-Imbrium craters large enough to penetrate the thick Imbrium deposit are rare to absent in the vicinity of the Apollo 16 site, however, so gardening mainly just rearranges the materials of the Imbrium deposit with little addition of post-Imbrium or post-Orientale material.

The modeled present stratigraphy of basin deposits at the Apollo 16 site, then, is (top downward) Imbrium, Serenitatis, and Nectaris deposits, with no extant Orientale deposit, an unconformity between the Serenitatis and Nectaris deposit where the Crisium and Humorum deposits were excavated by the Serenitatis event, and local unconformities where the subsequent basin-forming event may have excavated through the thinner regions of the Serenitatis and Nectaris deposits. The predicted present thicknesses of these deposits depends on the actual distribution of locations of deposit thicknesses within the SOI, and that is stochastic and cannot be predicted by the model. Thus, different locations within the present thickness of the Serenitatis deposit could presumably range from as much as ~2 km (thickest Serenitatis region attacked by relatively small Imbrium PriFrags, to nil (thin Serenitatis region attacked by larger Imbrium PriFrags). Similarly, the present Nectaris deposit thickness could presumably range from ~1.4 km to nil, depending on the areal distribution within the SOI of the original Nectaris deposit and the locations within the SOI of the craters produced by the larger Serenitatis PriFrags.

The modeled Imbrium deposit is presumably so thick that it would have been the only *deposit* sampled at the Apollo 16 site, but Imbrium ejecta would likely not have been the predominant material sampled. The *average* provenance makeup of the material in the Imbrium deposit is predicted by the model to be 18% Imbrium PriFrags, 21% Serenitatis PriFrags, 2% Crisium PriFrags, 0.3% Humorum PriFrags, 19% Nectaris PriFrags, and 40% pre-Nectarian substrate. Note that, given the ≥0.5 km thickness of the Imbrium deposit, North Ray Crater (1 km diameter) would not have excavated into the Serenitatis or the Nectaris deposit, in apparent contrast to some other models based on photogeology and samples (Spudis 1984; Stöffler et al. 1985). Although the material ejected by North Ray Crater would technically be part of the Imbrium deposit, at the small scale of that crater, the ejected materials could be dominated by feldspathic materials from an earlier part of the stratigraphic sequence, for example, from the Nectaris deposit (the Descartes Formation?) or the pre-Nectarian local substrate.

A challenge for the geochemist and petrologist is to determine the provenances of the various materials collected at the Apollo 16 site, a difficult task for which the results of the modeling are potentially useful. The predictions of the modeling are gross scale only; the deposits are not expected to be homogeneous on an intermediate or small scale, with some residual heterogeneities perhaps as large as kilometers. The composition of actual materials sampled may thus deviate substantially from an average provenance makeup. On a statistical basis, however, substantial deviations from the average deposit composition should not be the rule for all Apollo and Luna sampling sites.

A challenge for the photogeology and remote sensing community is to be aware of the modeled stratigraphy, and if deviations from it are substantial, to help us understand why the predictions of the model may have failed to provide a better description of the geology. Large-scale heterogeneity in the distribution of basin ejecta can be one major cause of discrepancies. Alternatively, the model may not apply because a basin-forming event was too oblique, or there may be some other, currently unsuspected reason for deviations. In cases of disagreement between model predictions and petrologic, geochemical, and photogeologic and remote sensing observations, however, it should be borne in mind that general observational evidence requires that large quantities of material were excavated from basins, that material had to go somewhere, and modern crater scaling is the best currently available estimate of its expected distribution.

### *The Orientale Basin*

Moore, Hodges, and Scott (1974) estimated the thicknesses of ejecta deposits associated with the Orientale Basin using three methods based on crater fill and rim heights (see Pike 1972). Two estimates were made for most locations, and the deposit thicknesses they obtained at each location depended on which method they used. Estimates based on filled craters average 3.0 ± 0.6 times those based on rim heights, and estimates based on partially filled craters average 1.8 ± 0.6 times those based on rim heights (arguably, ejecta might be more readily trapped in craters). The thicknesses of Orientale ejecta predicted by our model (b = 0.85, 45° ejection angle) are compared with the thicknesses estimated by Moore, Hodges, and Scott in Fig. 6. The standard parameters of Table 2 were used (except for d/D, which makes a small difference in maximum PriFrag sizes and has only a small effect on the results). The parameters of the Orientale excavation crater, based on gravity modeling of missing crustal mass (Wieczorek and Phillips 1999), are a radius of 198 km and a d/D of 0.13. The modeled deposit thicknesses (not shown) based on $\mu_{init}$ (as defined above) cover only the lower part of the range of the estimates of Moore, Hodges, and Scott as based on rim heights. The thicknesses based on $\mu_{eff}$ with DM = 3 cover nearly all of the estimates based on rim heights and the majority of those based on partly filled craters. The CL50% value passes through

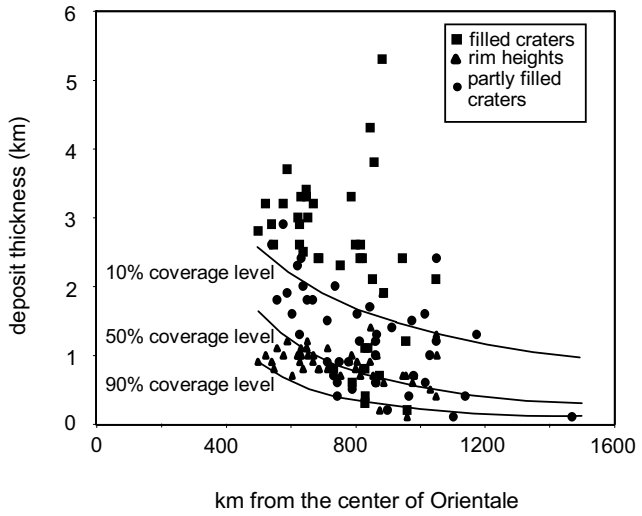


Fig. 6. Using three separate methods (which did not give mutually consistent results), Moore, Hodges, and Scott (1974) estimated the thicknesses of Orientale ejecta deposits as a function of distance from that basin (solid symbols). Modeled thicknesses are shown for the Orientale transient crater radius (lines). These observed Orientale deposit thicknesses were used (along with Ries deposit thicknesses) to calibrate an effective excavation depth parameter of the model (DM), so the apparent agreement of the model thicknesses with the Orientale thicknesses is not an independent result.

a region with a high density of points.

In fact, we use this result as a calibration to obtain the value for the depth multiplier of DM = 3 (above, and Equation 14). Some caveats apply. If the standard parameters of Table 2, the value of $\mu_{init}$, but a transient crater radius of 300 km are used, the CL10% to CL90% range also includes many of the data points with DM = 1. A radius of 300 km is near the upper limit of the values given by Spudis (1993). This shows the sensitivity of the model estimates to the presumed transient crater radius. Also, it should be remembered that because the ejection and secondary cratering process is stochastic, the 10% to 90% coverage level range is only the average range, and we may reasonably expect deviations in both directions outside of this range, and perhaps a factor of two in the direction of lower thicknesses, which may occur in locations reached by fewer than the average number of PriFrags. Deviations toward higher thicknesses require either larger PriFrags than appears reasonable, or a much higher or lower than expected surface density of relatively large PriFrags in the deposit at that location (e.g., because of azimuthal variation caused by an oblique impact), or unmodeled effects of lateral transport and trapping of ejecta.

We also point out that basin excavation cavities restored by Wieczorek and Phillips (1999) were done by simple vertical adjustment of the crustal column. Inward collapse, however, is of paramount importance to highly flattened and "megaterraced" ring basins (e.g., O'Keefe and Ahrens 1993, 1999). When post-impact crustal stratigraphy is adjusted by

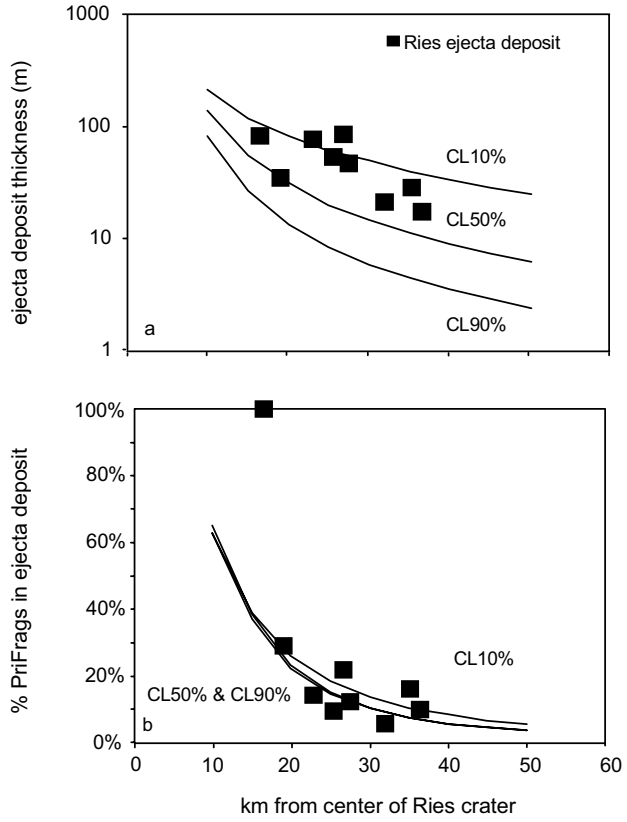


Fig. 7. Hörz et al. (1983) estimated thicknesses of the Bunte Breccia as a function of distance from the Ries impact structure (solid symbols). Using the same value for the excavation depth multiplier (DM = 3) as for the Orientale deposit thicknesses, the modeled Ries deposit thicknesses (lines) for CL10% to CL50% span most of the observed thicknesses. The modeled proportion of PriFrags in the ejecta matches the observed proportions well. This agreement can be considered independent confirmation of the calibration based on the Orientale results (Fig. 6), or it can be regarded that both the Orientale and the Ries deposit thicknesses were used to calibrate DM.

outward "back transport" of crustal material, the excavation cavities of Wieczorek and Phillips (1999) are larger, and our DM value for Orientale would be somewhat smaller than 3.

### *The Ries Crater*

Hörz et al. (1977, 1983) have provided deposit thicknesses and proportions of PriFrags based on several drill cores from the 26 km diameter Ries Crater, Germany. The modeling results for this well-studied crater furnish a further test of our model, including the calibration of the value of DM, and for another planet. The number of cores is small, so substantial scatter in the data can be expected and is observed. Hörz et al. suggest on geophysical grounds an excavation cavity radius of 6.5 km and an ejected volume of 150 (+50, –26) km$^3$. We used a radius of 6.5 km for our modeling. To extract 150 km$^3$ from a crater of that radius requires a relatively high value of d/D = 0.19 for the excavation cavity. This value of d/D does not affect the modeled thickness of the

ejecta deposit, because that parameter does not appear in Equation 7; it only affects the estimated size of the largest PriFrag ejected, making it, for example, a 150 m diameter sphere instead of a 120 m sphere at 20 km from the center of the Ries Crater, and that has only a small effect on the modeling.

As was the case for the Orientale deposit thicknesses, the best results from our modeling of the Ries deposits are obtained using a value of DM ~3. Results based on this value are compared with observations made on these cores in Fig. 7. Model estimates for %PriFrags in the deposits are excellent and are not a sensitive function of coverage level (Fig. 7). Model estimates for deposit thicknesses are toward the low side, with most observed values lying between the CL10% and the CL50% values. Equation 7, when used with a radius of 6.5 km and d/D = 0.10, corresponds to a smaller volume of ejecta than suggested for the Ries transient crater by Hörz et al. The deposit thickness can be improved by increasing the crater radius to 7–8 km, still retaining the 150 $km^3$ volume, but the %PriFrags increases as the crater radius is increased, resulting in a poorer fit to those observations. No combination of values of d/D, DM, and crater diameter tested significantly improved the quality of the match between the modeled and observed results from that of Fig. 7.

Morrison and Oberbeck (1978) calculated $\mu_{Ober}$ values of ~0.3 to 1.5 for Ries secondary craters (their Fig. 5). Their estimates of the proportion of local material (substrate) in the deposits are lower than most of the observed values (their Fig. 6). Their estimates of deposit thickness cross the field of data but are not a compelling fit to those data (their Fig. 7). Our $\mu_{eff}$ values range from 2.9 (CL10%) to 3.5 (CL50% and CL90%) at 20 km from the center of the Ries Crater, and are somewhat higher than the $\mu_{ober}$ values. Our $\mu_{eff}$ values range from 18 (CL10%) to 29 (CL50% and CL90%) at 50 km. The higher $\mu_{eff}$ values give a better fit to the Ries data than the $\mu_{ober}$ values.

Overall, the model reasonably predicts the observed deposit thicknesses in both the Orientale and the Ries cases using the same values for model parameters (except for g), including the same value of DM = 3. The model predicts %PriFrags for the Ries deposits very well. We thus conclude that the model can be a useful guide to deposit thicknesses for large-crater and basin-scale cratering. Even at an uncertainty level of perhaps a factor of two, the modeling provides useful insights into the characteristics of ejecta deposits, including rough estimates of their variability over the anticipated range of a geologic traverse. Also, we may expect that uncertainties of modelled characteristics for one location relative to another for a given impact event, or at one location affected by two or more different events, will be less than the absolute error of the model.

## Comparison of Model Predictions With Observed Crater Counts

Individual PriFrags produce secondary craters during ballistic sedimentation. The model takes into account the distribution of PriFrag sizes, and it is thus possible in theory to estimate the expected densities of secondary craters outside of the continuous ejecta deposit as a function of their size and their distance from the primary crater. As will be seen, the density and size distribution of observed secondary craters do not match our model expectations for ballistic sedimentation.

### *Crater Counts; Copernicus Secondary Craters*

We have already discussed the observed number of Copernicus secondary craters per SOI with diameters ≥0.5 km for the Copernicus ejecta deposits as a function of distance from the crater over the range tested (Figs. 1 and 2; Table 1). The number of observed and modeled secondary craters is compared in Fig. 2. The error bars on the observed points are ±1 standard deviation of the mean SOI crater count at each distance. This serves as a rough indication of the observed variability around the average. There is almost no change in the average number of secondary craters observed per SOI (15 × 15 km) over the range of distances for which the counts were made, and that result would not be expected if the process that produced the secondary craters is as modeled here. Results of the modeling for three PriFrag ejection angles (45° to 55° preferred, Cintala, Berthoud, and Hörz 1999) are shown in Fig. 2. The crater counts predicted for the ejection angle of 35° barely touch the error bar for the observed number of craters per SOI at 190 km. These results indicate that the model does not yield the correct number of *observed* secondary craters. This topic is further discussed below. We note that the modeled %PriFrags in the deposits at 150 km from the center of Copernicus is ~11%, compared with ~20–25% obtained by Pieters et al. (1985) on the basis of spectral data.

The calculations were done assuming that the secondary craters were formed in the gravity regime. The Copernicus secondary craters, which penetrated basalt flows, may have formed under conditions that lie in the broad transition region between gravity and strength modeling (e.g., Holsapple 1993). The modeling shown in Fig. 2 does not take this transition into account. Even for a hard material such as basalt, however, the gravity regime should hold for lunar craters of more than ~250 m in diameter (see Fig. 7 in Chapman and McKinnon 1986). If the material strength of coherent basalt is presumed ($A_s = 0.1$ and Y = 7 MPa, from Holsapple 1993, his Fig. 6.9 for hard rock, which suggests a transition diameter of ~3 km for the Moon), and gravity is ignored, the modeled crater density for Copernicus secondary craters at 150 km is still ~80% that of the gravity case and still much greater than the observed density. Using the value of 18 MPa also given by Holsapple (1993, his Table 1) does not significantly improve the model estimates relative to the observed crater counts.

### *Crater Counts; Imbrium and Orientale Secondary Craters*

Wilhelms, Oberbeck, and Aggarwal (1978) counted

Imbrium and Orientale secondary craters as a function of crater diameter over a range of ~1800 to 3600 km from the center of Imbrium (or ~5–10 transient crater radii, which includes the same range as for the Copernicus crater counts). Our model estimates of secondary crater density for the Imbrium event are compared with their observations in Fig. 8. We assumed the mature craters observed by Wilhelms, Oberbeck, and Aggarwal to be ~1.5 times their original diameters to account for collapse and longer-term mass wasting, and we have plotted them using the estimated transient crater radii. This exaggerates the probable expansion from the excavation cavity, and was done to favor the comparison with the results of the modeling. Even allowing this favorable exaggeration, the model, used with standard parameters (Table 2), including b = 0.85, gives crater densities that are an order of magnitude greater than the observed crater densities (Fig. 8). Note that these model densities also exceed the saturation-equilibrium values for crater density (e.g., Melosh 1989, his Fig. 10.2). The slope of the modeled crater size distribution is also substantially different from that of the observed crater size distribution. The largest model transient crater is ~7.5 km, far short of the 20 km maximum transient diameter for observed secondary craters (~30 km observed, adjusted to a 20 km approximate transient crater radius).

The modeled number of larger transient craters can be substantially reduced by changing the PriFrag distribution so that a higher fraction of the ejected primary material is in smaller PriFrags. This is achieved by raising the value of the b parameter in Equations 1 and 2. Estimates based on values of b in the range of 1.0–1.10 produce crater size distributions that cross the observed distribution, but no single value of b provides estimates that resemble the observed distribution, nor is there independent evidence to support the use of a value of b as high as 1.10.

Another means of changing the size distribution of modeled secondary craters is to change the minimum value of the velocity, $V_{min}$, in the cutoff for maximum PriFrag size, but the effect is small, as shown in a later section. Ejecta fragments substantially larger than the velocity-dependent cutoff allows seem to be required to produce the observed secondary craters, but the existence of such large PriFrags with high velocities is contrary to expectations because of the strain rate the high velocities would place on large ejected fragments (O'Keefe and Ahrens 1987, based on the theory of Grady and Kipp 1980). Schultz and Gault (1985) and Vickery (1986) considered the possibility that large fragments might arrive at a site of secondary impact in the form of clusters. Such clusters produce large diameter craters, but according to Schultz and Gault, they do not excavate as deeply as would a single impactor of the same mass or produce secondary craters with the same morphology as those produced by single impactors. Vickery rejected the cluster mechanism as an explanation for

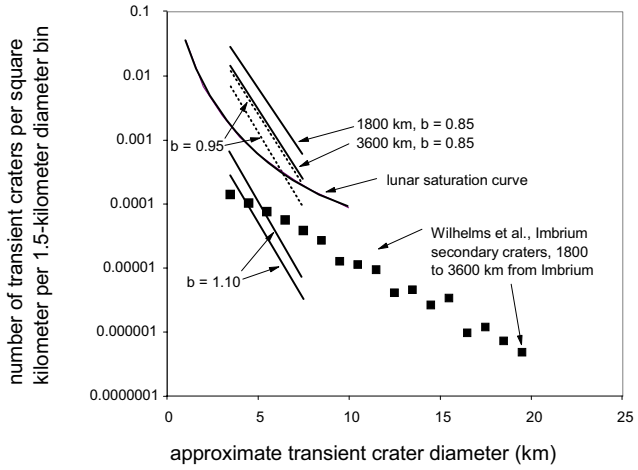


Fig. 8. This figure compares the results of our modeling with literature data on secondary crater counts. Data are for secondary craters of different sizes mainly within a range of ~1800 to 3600 km from the center of the Imbrium basin (Wilhelms, Oberbeck, and Aggarwal 1978), binned here at 1.5 km intervals of calculated transient crater diameter. The lunar saturation curve is from Melosh (1989, Fig. 10.2), also adjusted to approximate transient crater diameters for plotting here. Model estimated densities of Imbrium secondary craters are shown for three values of the primary fragment size distribution exponent b. The upper curve of each pair is the crater density expected at 1800 km from Imbrium, and the lower curve, that expected at 3600 km. It is evident that the model does not account for observed secondary craters. The model results in this figure were obtained using $V_{min}$ = 0.53 km/s and c = 2.0.

mainstream secondary craters, and we also observe that it does not appear to provide the necessary density and morphology of the larger secondary craters.

Vickery (1986), besides observing the decrease in maximum block size as a function of distance from lunar craters, recognized that large secondary craters at substantial distances from the primary craters required impactors far larger than the largest blocks she observed on crater rims. She attributed these secondary craters to the ejection of near-surface spallation fragments (see also Melosh 1984 and 1989, sections 5.4 and 6.4). In this interpretation, the large blocks necessary for production of secondary craters are ejected from shallow depths at a high velocity and do not receive the same strain rate as materials from greater depths. They act either as coherent blocks or as tight clusters of impactors to produce the large secondary craters. Vickery estimated that only ~0.7% of the Copernicus crater volume would be required to produce the secondary craters, within the estimated limits given by Melosh. The process as described by Melosh (1989, section 6.4, p. 107), however, indicates that spall plates will break apart if ejected at velocities exceeding ~0.5 km/s. The velocity required to move PriFrags from the Imbrium basin over a distance of 1800 km is >1.3 km/s. This calls into question whether the spallation mechanism can account for the large Imbrium secondary craters, at least as presently understood.

*Crater Obliteration During Ballistic Sedimentation*

If our model as outlined above, based on ballistic sedimentation and taking into account a distribution of PriFrag sizes, has merit, then we should expect a far higher density of secondary craters to have formed than is observed and their maximum diameter should be less than observed (modeled maximum of 7.4 km in transient crater diameter, ≤11 km final diameter, for Imbrium secondary craters in the distance range 1800–3600 km analyzed by Wilhelms, Oberbeck, and Aggarwal 1978). The expected density of PriFrags is high, and the PriFrags carry substantial forward momentum. This gives rise to a surge of debris in the downrange direction through mutual interference of secondary crater ejecta, and this has been described by Oberbeck (1975) and Oberbeck et al. (1975). This density of PriFrags, all falling rapidly onto the SOI, could result in obliteration of most if not all of the secondary craters whose formation produces the surge (also discussed by Oberbeck et al.).

Our model calculations also suggest that obliteration should be extensive. For example, at a distance of 1800 km from the center of the Imbrium basin (the minimum distance for Imbrium secondary craters as observed by Wilhelms, Oberbeck, and Aggarwal 1978), according to our model, using b = 0.85, the SOIs are half saturated (CL50%) with craters 2.6 km in (transient crater) diameter and larger and 90% saturated (CL90%) with craters 1.2 km in diameter and larger. As individual craters, these would be excavated to maximum depths of 260 m and deeper and 120 m and deeper by the PriFrags that produced them (based on $\mu_{indiv}$), but some would be excavated to three times those depths, ~780 and 360 m and deeper, based on $\mu_{eff}$, which corresponds to the depths of scouring by all the PriFrags falling on the SOI within those coverage levels. These greater depths of excavation are equivalent to maximum depths that would be reached by individual modeled craters ($\mu_{indiv}$) of diameters 7.8 km and 3.6 km. Excavation to depths of 780 and 360 m by craters at CL50% and CL90% suggests that the debris surge produced by ballistic sedimentation would virtually eliminate individual craters of 3.6 km diameter and eliminate or modify those of 7.8 km diameter. The maximum size of transient crater produced at 1800 km according to our model would be ~7.4 km. Thus, few if any secondary craters produced during the surge should survive the surge, and those that do should show significant degradation. Even where the PriFrag surface density is the lowest (~3500 km, near the 3600 km limit of the survey of Wilhelms, Oberbeck, and Aggarwal), the surge would virtually eliminate craters in the ≤7.2 km diameter size range, the largest size produced at that distance according to our model. In short, the surface densities of kilometer-sized secondary craters are so high that mutual crater obliteration would be rampant, and probably would be virtually complete when the surge had passed its peak of intensity. This seems to require that the secondary craters formed at the end of the surge or after it had ended.

Similarly, for Copernicus, according to our model (b = 0.85, 45° launch angle), at a distance of 145 km, or 4.7 transient crater radii (or roughly one crater diameter beyond the edge of the continuous ejecta deposit), depths of excavation range from 170 m at CL10% through 26 m at CL90%. Corresponding deposit thicknesses are 320 m and 30 m. PriFrag impacts should thus obliterate most craters produced during the surge that are 0.3 km in diameter and some or many craters that are ~1–2 km in diameter. The largest crater size produced according to the model is 0.9 km in diameter and the CL10% crater is 570 m in diameter, so essentially all secondary craters associated with the main surge would be obliterated.

These estimates of crater obliteration are based on an azimuthally symmetric distribution of PriFrags, and are intended to show that PriFrag bombardment is so intense that most craters associated with the surge would be obliterated. PriFrag distributions are in fact not azimuthally symmetric; deposit thicknesses vary, and some areas have rays while others do not. The point is this: Far more secondary craters are expected to form than are observed or than could be expected to survive the intense bombardment.

Unless the ejection angles and velocities of PriFrags reaching a given spot are all the same, not all PriFrags will arrive there simultaneously. For example, Imbrium PriFrags ejected at 45° and having velocities of 1.30 km/s reach the Apollo 16 site, and those ejected at 55° with velocities of 1.40 km/s also reach that site. Although ejected earlier, the PriFrags ejected at the steeper 55° angle arrive later. Flight times are some 11 minutes different, more than enough time for a peak debris surge produced mainly by ~45° PriFrags to abate. Earlier ejection of the 55° PriFrags would have little effect on the relative arrival times, given that the time to produce the entire Imbrium transient crater may be as little as 2–3 minutes (Melosh 1989, Section 7.11). Some observable secondary craters might thus be formed by late-arriving PriFrags that are part of the main ejecta. This mechanism cannot account for the larger secondary craters, however. Whatever mechanism is responsible for secondary crater formation seems to require large PriFrags ejected at somewhat steeper angles so that the surge has concluded prior to their arrival. This analysis suggests that there is much yet to be learned about secondary crater formation accompanying large impacts.

## Effects on Model Results of Varying the Values of Some Input Parameters

In the modeling results shown so far, values of most input parameters have been held constant. Here, we describe the effects of changes in values, using the Imbrium event as the illustration. The "nominal" set used for most calculations is shown in Table 2. When effects of one parameter value were tested, nominal values were used for the rest.

*Ejecta Launch Angle*

Arguments have been presented in favor of ejecta launch

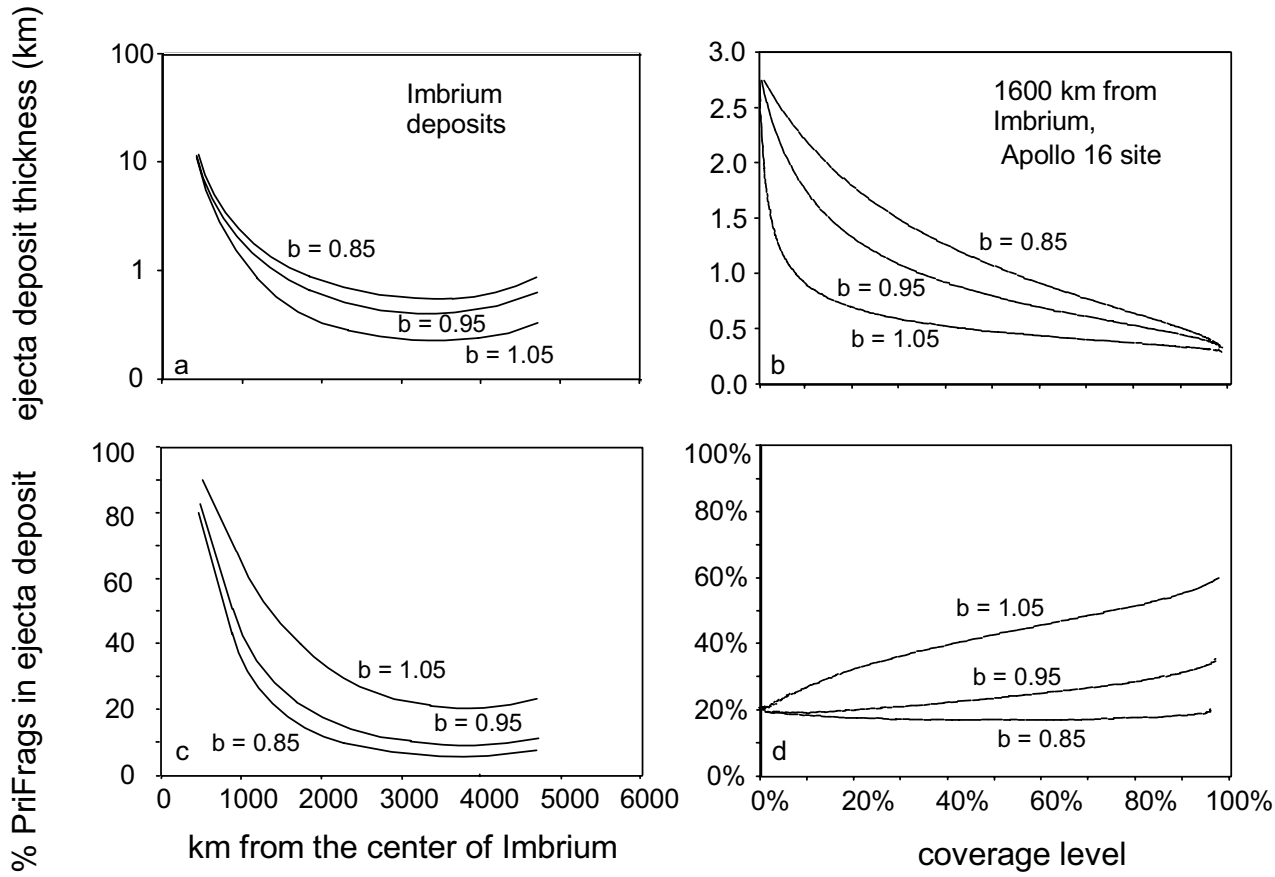


Fig. 9. Effects are shown of changing the relative proportions of PriFrags of each different size (the fragmentation factor b, Equation 1) for the case of the Imbrium event as a function of distance from the center of the Imbrium basin and as a function of the coverage level at the Apollo 16 site (1600 km from the center of the Imbrium basin). Differences become large as b approaches or exceeds unity and the distribution becomes more strongly weighted toward a higher fraction of the mass in smaller PriFrags.

angles ranging from ~15°, as measured from the horizontal (e.g., Shoemaker 1962; Oberbeck and Morrison 1974), to 55° or more (e.g., Vickery 1986; Cintala, Berthoud, and Hörz 1999; O'Keefe and Ahrens 1999). Recent laboratory results for sand showed a range from ~55° for ejecta from near the center of the crater to 45° for those farther out (Cintala, Berthoud, and Hörz 1999). The effects of changing the ejecta launch angle for the Imbrium event are shown for the ejecta deposit thickness and the %PriFrags in the deposits as a function of distance at CL50% (Fig. 4), and they are shown as a function of coverage level at 1600 km from the center of Imbrium (the distance of the Apollo 16 site; Fig. 5). The effect on deposit thickness of changing the angle by ±10° from the nominal angle of 45° is ~30% where the maximum difference occurs, at ~3500 km from the center of Imbrium. The fractional change in %PriFrags is less, ~15% where the maximum difference occurs, at ~3800 km. At 1600 km, the effect on deposit thickness of changing the ejection angle by 10° from the nominal 45° is 16–23% at CL50%. The effect on the %PriFrags is 9–20%. These differences are smaller than we can presently measure. The effect of changing the ejecta launch angle on modeled Copernicus crater counts was shown in Fig. 2.

*Fragmentation Exponent b*

As was discussed in a previous section, the output of the model is affected substantially by the value used for the fragmentation exponent b (Equation 1), which determines the size distribution of the PriFrags. Except as indicated in Fig. 8, we have used a value of 0.85 in our calculations, in agreement with impact cratering experiments (Turcotte 1992). The effects of changing b in the model for the Imbrium event are shown as a function of distance and for different coverage levels at the distance of the Apollo 16 site in Fig. 9. Over the range $0.85 < b < 0.95$, effects on both deposit thickness and %PriFrags are relatively small. As b approaches and exceeds unity, however, the magnitude of the effect increases and continues to increase as the size distribution becomes more heavily weighted in favor of smaller PriFrags. High values of b significantly increase the fraction of PriFrags in the ejecta deposits. Fewer deeply excavating large PriFrags are available to excavate high fractions of the SOI, and more smaller

PriFrags are available to mix with a smaller amount of substrate. If, as suggested by some investigators (e.g., Shoemaker 1965; Garvin 1990), the bulk of the mass is carried by smaller rather than larger PriFrags (i.e., b ≥1.0), then ejecta deposits would be more shallow on average and more PriFrag-rich than our modeling suggests. Note also that the modeling results are necessarily sensitive to the lower mass limit selected for PriFrags when the value of b exceeds 1.0. At CL50%, b = 1.1, a 45° launch angle, a lower mass limit of 1 μg gives %PriFrags ~20% higher and a deposit thickness ~15% lower than the lower mass limit of 0.1 g used in the modeling in this paper.

*Maximum PriFrag Size*

The exponent c determines the rate at which the maximum PriFrag size decreases with PriFrag velocity; the effects of changing c on both ejecta deposit thickness and the proportion of PriFrags in the ejecta deposits are relatively small, as shown in Fig. 10. The greatest effects on deposit thickness occur at the lowest coverage levels, for which the deep excavations of the largest PriFrags are prominent (Apollo 16 site, Fig. 10c). Changing the value of $V_{min}$ for Imbrium from 0.53 to 0.65 km/s has a relatively small effect. Thus, in our modeling we have used 0.53 km/s for $V_{min}$ (Imbrium) and −2.0 for c.

*Depth/Diameter and Mass Balance*

Deposit thicknesses and %PriFrags depend on the mass of PriFrags falling on an SOI. As pointed out by others, e.g., Moore, Hodges, and Scott (1974) and Pike (1974), the early procedure of McGetchin, Settle, and Head (1973) falls considerably short of providing mass balance if the primary excavation crater is taken as a paraboloid with depth to diameter of 0.1. Nor does their formula for ejecta thickness obey geometric similarity, as it should (see Housen, Schmitt, and Holsapple 1983). The effects of changing the depth to diameter ratio by ±0.05 from the nominal value of 0.10 would be substantial because that is tantamount to changing the value for the A parameter in Equation 7. Changing the mass ejected from a basin in this way does not proportionately change the deposit thickness or the %PriFrags, however. For example, increasing the total mass ejected results in a higher surface density of larger PriFrags at a given distance from the primary crater. The larger PriFrags control the coverage levels, and thus increase the crater diameter associated with any coverage level, even though the PriFrag size distribution and PriFrag velocity remain constant. For our modeling, we have assumed a depth to transient diameter ratio of 0.1, except as noted for the Orientale and Ries Craters. As used here, however, the value of d/D affects the size of the largest PriFrag reaching an SOI and deposit thickness, as discussed above for the Ries Crater.

We tested the effects of changing each of the empirical constants in Equation 7, while holding the others at their nominal values. The constant A is essentially a multiplier, and the effects are roughly proportional to the change in its value. Using the nominal value of A = 0.2 provides approximate mass balance for a paraboloid excavation crater with d/D = 0.10 less 10%, as described above (certainly within the uncertainty of the amount of ejecta near the rim). Given that mass balance and noting the underestimate by Equation 7 of deposit thickness very close to the rim of the primary crater (Housen, Schmitt, and Holsapple, their Fig. 8), we see that the value of 0.20 for A may somewhat overestimate the amount of more distal ejecta, a possibility difficult to evaluate for basin-sized impacts. Changing the value of $e_r$ has more subtle, small effects. For the SOI ring at 1600 km, changing the value of $e_r$ from 2.5 to 3.5 causes only insignificant changes in deposit thickness or the fraction of PriFrags. Changes in these parameters should not be made individually, however, as discussed below.

*Overall Effects of Parameter Choices*

The values for the various parameters have been evaluated above as if each were independent of the others. Were this the case, then by selecting extreme values for the individual parameters, extreme results from the modeling would be obtained. Such a selection would be inappropriate because the values of individual parameters are determined empirically as parts of sets of values for a particular experiment or group of experiments. The allowable range of model results is thus constrained by sets of interdependent parameter values. Overall, we estimate that effects of allowable parameter variations, uncertainties associated with extrapolating laboratory and explosion data to basin-forming impacts, and imprecision in testing model predictions against basin ejecta properties limit the error of the modeling to not more than a factor of two for deposit thickness and somewhat less for the fraction of PriFrags. A more quantitative assessment of errors for basin ejecta modeling cannot be made at this time.

The particular choices of nominal parameter values used here can be disputed. The general results of the modeling are nevertheless robust to reasonable variations in the values used for these parameters. Indications from the literature on cratering and ejecta scaling are that the large quantities of ejecta described by the model are correct and that the distribution of that large quantity of material with distance from the impact site does occur as indicated. Thus, the consequences at a lunar site for sample collection and remote measurements of the deposit thicknesses and fraction of PriFrags predicted by the model deserve serious consideration. If our inferences on ejecta deposits are wildly erroneous, then one or more of the present concepts of ejecta scaling (including fragment size distribution), transient crater cavity dimensions, and ejected volumes must be awry.

A more sophisticated model could be developed. For instance, models that incorporated the relationship between

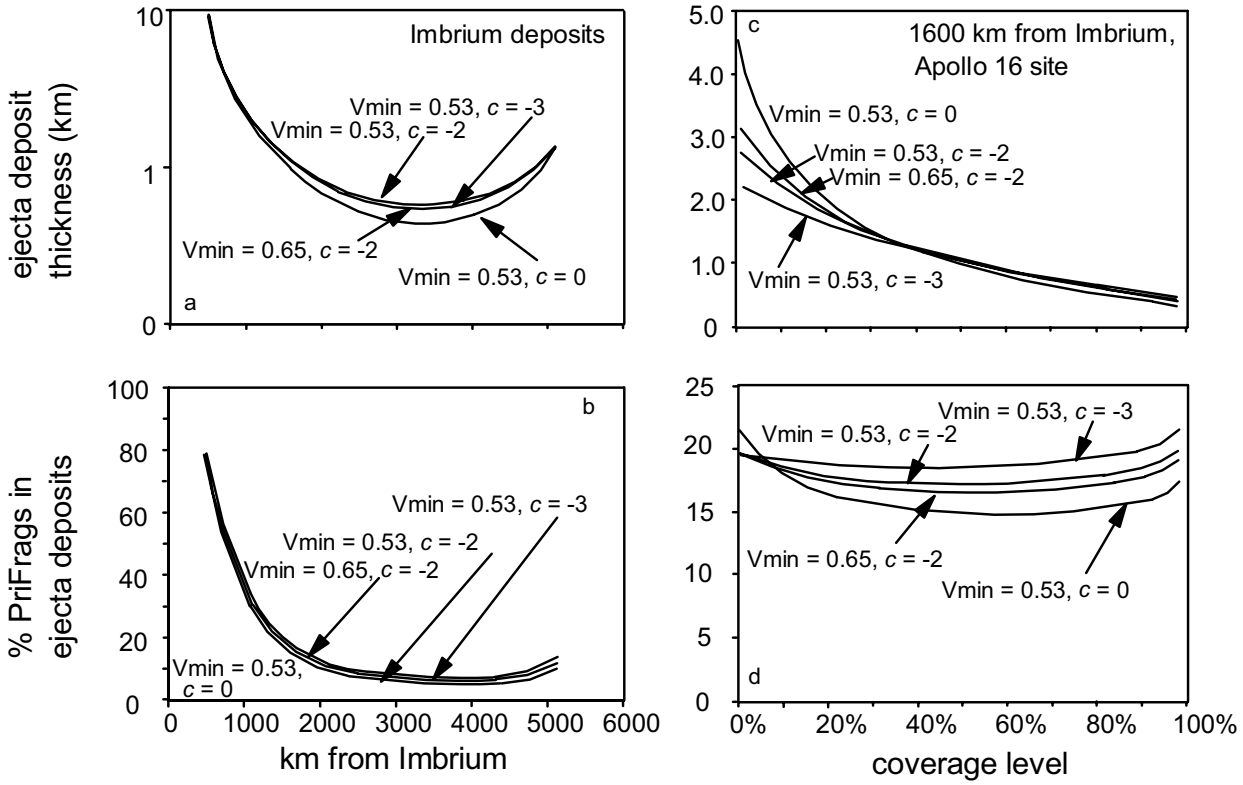


Fig. 10. a, b) Effects are shown of changing the values of the parameters in the equation for decrease of maximum PriFrag size with velocity (or with distance from the primary crater, in this case, Imbrium). A value of zero for the exponent c keeps the size distribution of PriFrags constant at all distances. This results in the shallowest deposits and the lowest fraction of PriFrags in the deposits. This can be understood in the example at one location in panels c and d. At the lowest coverage levels, the larger PriFrags for c = 0 dig deeper than the largest PriFrags for c = 2 or 3, and the c = 0 deposits are thicker than the c = 2 or 3 deposits. Also, because the excavation efficiency for large PriFrags is lower than for smaller PriFrags, the deepest deposits have higher %PriFrags. At higher coverage levels, the medium sized PriFrags for c = 0 are fewer and a little smaller than the c = 2 or 3 PriFrags, and the c = 0 deposits are shallower and less PriFrag rich. Except at the lowest coverage levels, the effects are relatively small.

ejecta velocity and launch position, systematic changes in ejecta angle with velocity, or used a stochastic distribution of ejecta angles, would be supported by the literature. The observational constraints on ejecta deposits from basins or large craters currently available are not sufficient to warrant a more sophisticated approach, but we encourage the gathering of new data and numerical simulation of the ejection process. Most importantly, relative values for different impacts based on the same parameter choices are defendable, and no reasonable choices of parameter values will greatly alter the broader conclusions reached on the basis of those comparisons. All the parameter options considered here gave roughly similar results, the largest differences being produced by changes in the PriFrag mass distribution exponent b.

No choice of parameter can bring the model results into line with observed secondary crater densities and diameters. Production of secondary craters appears to require a separate mechanism and presumably a mechanism that produces them subsequent to the ground surge that is associated with ballistic sedimentation.

## CONCLUSIONS AND SUMMARY

1. We have developed a quantitative model that estimates probabilities for average properties of ejecta deposits deriving from a primary impact event. This model, largely a concatenation of existing models, is based on ballistic sedimentation (e.g., Oberbeck 1975) and on modern crater ejecta scaling (see reviews by Chapman and McKinnon 1986; Melosh 1989; Holsapple 1993). The probabilities obtained from the model are presented as variations in ejecta deposit properties within a "square of interest" (SOI) of any chosen size (e.g., a 100 × 100 km square centered on a location of interest such as an Apollo landing site). Quantities predicted by the model include deposit thickness and fraction of primary ejecta and pre-existing substrate incorporated into the ejecta deposit. The model also estimates the variation of these properties as a function of the fraction of the SOI considered. The model uses a form of excavation efficiency that does not allow every primary fragment to

act independently to excavate fresh substrate, and it calibrates the effective excavation efficiency to literature data on observed deposit thicknesses surrounding the Orientale basin and the Ries impact crater.

The results of the modeling bear on the provenances of materials at non-mare sampling or remote sensing sites. They can be used as a tool for planning robotic lander traverses and as a consideration in developing geologic interpretations. Results of the model are consistent with simple mass balance based on the geometry of the primary crater.

2. Predicted secondary crater densities are at least an order of magnitude greater than observed secondary crater densities surrounding the Imbrium and Orientale basins, and the slope of the modeled distribution of secondary craters as a function of their diameter is steeper than that observed for secondary craters. If the distribution of primary fragments is that expected from the modeling, then the bulk of the secondary craters that formed as part of the ballistic sedimentation process would have mutually obliterated each other. A mechanism appears to be required that produces the observed secondary craters after the main debris surge has subsided. Neither the ejection of primary fragments as formulated here nor spallation in its present theoretical form appears capable of producing basin secondary craters as large as are observed.
3. New data are provided for crater densities in the northern half of the Copernicus secondary crater field at distances of 4.7–6.8 transient crater radii (190–210 km). All 15 km × 15 km SOIs at that distance contain at least one secondary crater, and most do not deviate from the measured average value by as much as 50%. This suggests that modeled average properties of ejecta deposits may be reasonable guides to expected properties. As was the case for Imbrium and Orientale secondary craters, modeled densities for Copernicus secondary craters are much higher than observed crater densities.

*Acknowledgments*–This work benefited greatly from extensive and time-consuming informal and formal reviews by B. Cohen, M. Cintala, F. Hörz, V. Oberbeck, and V. Sharpton, which we acknowledge with great appreciation. R. Korotev, B. Jolliff, and J. Gillis provided helpful discussions and suggestions for improvement of the manuscript. This work was supported in part by the National Aeronautics and Space Administration under Grants NAG 4172 and NAG5-10485.

## REFERENCES

Andrews R. J. 1975. Origin and distribution of ejecta from near-surface laboratory-scale cratering experiments. Report AFWL-TR-74–314. pp. 207.

Chapman C. R., and McKinnon W. B. 1986. Cratering of planetary satellites. In *Satellites*, edited by Burns J.A. and Matthews M. S. Tucson: University of Arizona Press. pp. 492–525.

Cintala M. J., Garvin J. B., and Wetzel S. J. 1982. The distribution of blocks around a fresh lunar mare crater (abstract). 13th Lunar and Planetary Science Conference. pp. 100–101.

Cintala M. J., Berthoud L., and Hörz F. 1999. Ejection-velocity distributions from impacts into coarse-grained sand. *Meteoritics & Planetary Science* 34:605–623.

Dobrovolskis A. 1981. Ejecta patterns diagnostic of planetary rotations. *Icarus* 47:203–219.

Garvin J. B. 1990. The global budget of impact-derived sediments on Venus. *Earth, Moon, and Planets* 50/51:175–190.

Garwood F. 1947. The variance of the overlap of geometrical figures with reference to a bombing problem. *Biometrika* 34:1–17.

Gault D. E., Shoemaker E. M., and Moore H. J. 1963. Spray ejected from the lunar surface by meteoroid impact. NASA Technical Note D-1767.

Gault D. E., Guest J. E., Murray J. B., Dzurisin D., and Malin M. C. 1975. Some comparisons of impact craters on Mercury and the Moon. *Journal of Geophysical Research* 80:2444–2460.

Grady D. E. and Kipp E. 1980. Continuum modeling of explosive fracture in oil shale. *International Journal of Rock Mechanics and Mining Sciences and Geomechanics Abstracts* 17:147–157.

Hartmann W. K. 1969. *Moons & Planets*. 3rd edition. Belmont: Wadsworth. p. 510.

Haskin L. A. 1998. The Imbrium impact event and the thorium distribution at the lunar highlands surface. *Journal of Geophysical Research* 103:1679–1689.

Haskin L. A., McKinnon W. B., and Benner L. A. M. 1996. Could Imbrium ejecta be the source of the high-Th material in the Van de Graaff Region of the Moon (abstract). 27th Lunar and Planetary Science Conference. pp. 501–502.

Haskin L. A., Korotev R. L., Rockow K. L, and Jolliff B. L. 1998. The case for an Imbrium origin of the Apollo thorium-rich impact-melt breccias. *Meteoritics & Planetary Science* 33:959–975.

Haskin L. A., Korotev R. L., Gillis J. J., and Jolliff B. L. 2002. Stratigraphies of Apollo and Luna highland landing sites and provenances of materials from the perspective of basin impact ejecta modeling (abstract #1364). 33rd Lunar and Planetary Science Conference. CD-ROM.

Haskin L. A., Moss B. E., and McKinnon W. B. 1995. How much Imbrium material should be present at the Apollo 17 site (abstract). 26th Lunar and Planetary Science Conference. pp. 557–558.

Holsapple K. A. 1993. The scaling of impact processes in planetary sciences. *Annual Review of Earth and Planetary Sciences* 21: 333–373.

Holsapple K. A. and Schmitt R. M. 1982. On the scaling of crater dimensions 2. Impact processes. *Journal of Geophysical Research* 87:1849–1870.

Hörz F., Gall H., Hüttner R., and Oberbeck V. R. 1977. Shallow drilling in the "Bunte Breccia" impact deposits, Ries Crater, Germany. In *Impact and Explosion Cratering*, edited by Roddy D. J., Pepin R. O., and Merrill R. B. NewYork: Pergamon Press. pp. 425-448.

Hörz F., Ostertag R., and Rainey D. A. 1983. Bunte Breccia of the Ries: Continuous deposits of large impact craters. *Reviews of Geophysics and Space Physics* 21:1667–1725.

Housen K. R., Schmitt R. M., and Holsapple K. A. 1983. Crater ejecta scaling laws: Fundamental forms based on dimensional analysis. *Journal of Geophysical Research* 88:2485–2499.

Jolliff B. L., Gillis J. J., Haskin L. A., Korotev R. L., and Wieczorek M. A. 2000. Major lunar crustal terranes: Surface expressions and crust-mantle origins. *Journal of Geophysical Research* 105: 4197–4216.

McGetchin T. R., Settle M., and Head J. W. 1973. Radial thickness

variation in impact crater ejecta: Implications for lunar basin deposits. *Earth and Planetary Science Letters* 20:226–236.

Melosh H. J. 1984. Impact ejection, spallation, and the origin of meteorites. *Icarus* 59:234–260.

Melosh H. J. 1989. *Impact cratering*. Oxford: Oxford University Press. p. 245.

Moore H. J. 1971. Large blocks around lunar craters. In *Analysis of Apollo 10 photography and visual observations*. NASA-SP 232: 26–27.

Moore H. J., Hodges C. A., and Scott D. H. 1974. Multiringed basins—illustrated by Orientale and associated features. Proceedings, 5th Lunar and Planetary Science Conference. pp. 71–100.

Morrison R. H. and Oberbeck V. R. 1975. Geomorphology of crater and basin deposits—emplacement of the Fra Mauro Formation. Proceedings, 6th Lunar and Planetary Science Conference. pp. 2503–2530.

Morrison R. H. and Oberbeck V. R. 1978. A composition and thickness model for lunar impact crater and basin deposits. Proceedings, 9th Lunar and Planetary Science Conference. 3763–3785.

Moss B. E. and Haskin L. A. 1994. Toward systematic estimation of the origins of regolith materials that might be sampled during a lunar highland geologic traverse (abstract). 25th Lunar and Planetary Science Conference. pp. 943–944.

Oberbeck V. R. 1975. The role of ballistic erosion and sedimentation in Lunar stratigraphy. *Reviews of Geophysics and Space Physics* 13:337–362.

Oberbeck V. R. and Morrison R. H. 1974. Laboratory simulations of the lunar herringbone pattern. *Moon* 9:415–455.

Oberbeck V. R., Hörz F., Morrison R. H., Quaide W. L., and Gault D. E. 1974. Smooth plains and continuous deposits of craters and basins. Proceedings, 5th Lunar and Plantary Science Conference. pp. 111–136.

Oberbeck V. R., Hörz F., Morrison R. H., Quaide W. L., and Gault D. E. 1975. On the origin of lunar smooth-plains. *Moon* 12:19–54.

O'Keefe J. D. and Ahrens T. J. 1987. The size distributions of fragments ejected at a given velocity from impact craters. *International Journal of Impact Engineering* 25:493–499.

O'Keefe J. D. and Ahrens T. J. 1993. Planetary cratering mechanics. *Journal of Geophysical Research* 98:17011–17028.

O'Keefe J. D. and Ahrens T. J. 1999. Complex craters: Relationship of stratigraphy and rings to impact conditions. *Journal of Geophysical Research* 104:27091–27104.

Pieters C. M., Adams J. B., Mouginis-Mark P. J., Zisk S. H., Smith M. O., Head J. W., and McCord T. 1985. The nature of crater rays: The Copernicus example. *Journal of Geophysical Research* 80: 12393–12413.

Pike R. J. 1972. Geometric similitude of lunar and terrestrial craters. Proceedings, 24th International Geological Congress. pp. 41–47.

Pike R. J. 1974. Ejecta from large craters on the moon: Comments on the geometric model of McGetchin et al. *Earth and Planetary Science Letters* 23:265–274.

Schmidt R. M. and Housen K. R. 1987. Some recent advances in the scaling of impact and explosion cratering. *International Journal of Impact Engineering* 5:543–560.

Schultz P. H. 1998. Forming the South Pole-Aitken Basin: The extreme games (abstract). 29th Lunar and Planetary Science Conference. CD-ROM.

Schultz P. H. and Gault D. E. 1985. Clustered impacts: Experiments and implications. *Journal of Geophysical Research* 90:3701–3732.

Schultz P. H. and Mendell W. 1978. Orbital infrared observations of lunar craters and possible implications for impact ejecta emplacement. Proceedings, 9th Lunar and Planetary Science Conference. pp. 2857–2883.

Shoemaker E. M. 1962. Interpretation of lunar craters. In *Physics and Astronomy of the Moon*, edited by Kopal Z. New York: Academic Press. pp. 283–359.

Shoemaker E. M. 1965. Preliminary analysis of fine structure of the lunar surface in Mare Cognitum. JPL–NASA Technical Report 32-700:75.

Spudis P. D. 1993. *The geology of multi-ring impact basins*. New York: Cambridge University Press. pp. 263.

Spudis P. D. 1994. Apollo 16 site geology and impact melts: Implications for the geologic history of the lunar highlands. Proceedings, 15th Lunar and Planetary Science Conference. *Journal of Geophysical Research* 89:C95–C107.

Spudis P.D., Reisse R.A., and Gillis J.J. 1994. Ancient multiring basins on the Moon revealed by Clementine laser altimetry. *Science* 266:1848–1851.

Stöffler D., Gault D. E., Wedekind J., and Polkowski G. 1975. Experimental hypervelocity impact into quartz sand: Distribution and shock metamorphism of ejecta. *Journal of Geophysical Research* 80:4062–4077.

Stöffler D., Bischoff A., Borchardt R., Burghele A., Deutsch A., Jessberger E. K., Ostertag R., Palme H., Spettel B., Reimold W. U., Wacker K., and Wänke H. 1985. Composition and evolution of the lunar crust in the Descartes highlands, Apollo 16. Proceedings, 15th Lunar and Planetary Science Conference. *Journal of Geophysical Reserach* 90:C449–C506.

Turcotte D. L. 1992. *Fractals and chaos in geology and geophysics*. New York: Cambridge University Press. p. 221.

Vickery A. M. 1986. Size-velocity distribution of large ejecta fragments. *Icarus* 67:224–236.

Vickery A. M. 1987. Variation in ejecta size with ejection velocity. *Geophysical Research Letters* 14:726–729.

Wieczorek M. A. and Phillips R. J. 1999. Lunar multi-ring basins and the cratering process. *Icarus* 139:246–259.

Wieczorek M. A. and Zuber M. T. 2001. A Serenitatis origin for the Imbrian grooves and South Pole-Aitken thorium anomaly. *Journal of Geophysical Research* 106:27853–27864.

Wilhelms D. E. 1987. The geologic history of the Moon. U. S. Geological Survey Professional Paper 1348.

Wilhelms D. E., Oberbeck V. R., and Aggarwal H. R. 1978. Size-frequency distributions of primary and secondary lunar impact craters. Proceedings, 9th Lunar and Planetary Science Conference. pp. 3735–3762.